Translational Stroke Research
https://doi.org/10.1007/s12975-020-00810-3

ORIGINAL ARTICLE

TRPM7 Mediates Neuronal Cell Death Upstream of Calcium/Calmodulin-Dependent Protein Kinase II and Calcineurin Mechanism in Neonatal Hypoxic-Ischemic Brain Injury

Ekaterina Turlova[1,2] · Raymond Wong[1,2] · Baofeng Xu[1,2] · Feiya Li[1,2] · Lida Du[1,2] · Steven Habbous[2] · F. David Horgen[3] · Andrea Fleig[4] · Zhong-Ping Feng[2] · Hong-Shuo Sun[1,2,5,6]

Received: 8 August 2019 / Revised: 12 March 2020 / Accepted: 18 March 2020

Abstract

Transient receptor potential melastatin 7 (TRPM7), a calcium-permeable, ubiquitously expressed ion channel, is critical for axonal development, and mediates hypoxic and ischemic neuronal cell death in vitro and in vivo. However, the downstream mechanisms underlying the TRPM7-mediated processes in physiology and pathophysiology remain unclear. In this study, we employed a mouse model of hypoxic-ischemic brain cell death which mimics the pathophysiology of hypoxic-ischemic encephalopathy (HIE). HIE is a major public health issue and an important cause of neonatal deaths worldwide; however, the available treatments for HIE remain limited. Its survivors face life-long neurological challenges including mental retardation, cerebral palsy, epilepsy and seizure disorders, motor impairments, and visual and auditory impairments. Through a proteomic analysis, we identified calcium/calmodulin-dependent protein kinase II (CaMKII) and phosphatase calcineurin as potential mediators of cell death downstream from TRPM7 activation. Further analysis revealed that TRPM7 mediates cell death through CaMKII, calmodulin, calcineurin, p38, and cofilin cascade. In vivo, we found a significant reduction of brain injury and improvement of short- and long-term functional outcomes after HI after administration of specific TRPM7 blocker waixenicin A. Our data demonstrate a molecular mechanism of TRPM7-mediated cell death and identifies TRPM7 as a promising therapeutic and drug development target for HIE.

Keywords TRPM7 · Ion channel · Calcium/calmodulin-dependent protein kinase II · Calcineurin · Cofilin · Hypoxic-ischemic brain injury · Neuroprotection · Waixenicin A

Abbreviations

TRPM7 channel	Transient receptor potential melastatin 7 channel

Ekaterina Turlova and Raymond Wong contributed equally to this work.

Electronic supplementary material The online version of this article (https://doi.org/10.1007/s12975-020-00810-3) contains supplementary material, which is available to authorized users.

✉ Zhong-Ping Feng
zp.feng@utoronto.ca

✉ Hong-Shuo Sun
hss.sun@utoronto.ca

[1] Department of Surgery, Faculty of Medicine, University of Toronto, 1 King's College Circle, Toronto, Ontario M5S 1A8, Canada

[2] Department of Physiology, Faculty of Medicine, University of Toronto, 1 King's College Circle, Toronto, Ontario M5S 1A8, Canada

[3] Department of Natural Sciences, Hawaii Pacific University, Kaneohe, HI 96744, USA

[4] Center for Biomedical Research at The Queen's Medical Center and John A. Burns School of Medicine, University of Hawaii, Honolulu, HI 96720, USA

[5] Department of Pharmacology, University of Toronto, 1 King's College Circle, Toronto M5S 1A8, Canada

[6] Leslie Dan Faculty of Pharmacy, University of Toronto, University of Toronto, Toronto, Canada

Introduction

Transient receptor potential melastatin 7 (TRPM7) is a non-selective Ca^{2+}-permeable divalent cation channel [1, 2, 3] that has been implicated in a variety of neurodegenerative conditions including ischemic stroke [4], familial Alzheimer's disease [5], and neuronal cell death due to hydrogen peroxide and superoxide accumulation [6]. TRPM7 has been previously identified as a potential non-glutamate target for hypoxic-ischemic neuronal injury. In vitro suppression of TRPM7 using siRNA reduced anoxic neuronal cell death in culture [7], and in vivo suppression of TRPM7 via virally mediated siRNA in adult rats improved hippocampal neuron survival and neurobehavioral outcomes following global cerebral ischemia [4]. However, despite the recent progress in the field, the role of TRPM7 in neurons has remained largely phenomenal due to the lack of specific pharmacological modulators.

Calcium/calmodulin-dependent protein kinase II (CaMKII) is a well-known regulator of synaptogenesis, synaptic plasticity, learning, and memory. CaMKII activity has also been shown to be essential to neuronal survival and function. Under excitotoxic conditions, such as ischemic stroke, CaMKII has been shown to rapidly inactivate [8, 9]. In fact, the extent of brain damage after hypoxic-ischemic insult has been shown to closely overlap with the regions of CaMKII inactivation [8], while CaMKII α subunit knockout mice showed significantly greater infarct volumes following ischemia compared with their wild-type counterparts [10]. Several other studies showed that genetic and pharmacological inhibition of CaMKII may be associated with calcium homeostasis dysregulation, hyperexcitability due to disruption of glutamate signaling, and neuronal death [11, 12].

On the other hand, activation of calcium/calmodulin-dependent phosphatase calcineurin has been shown to be detrimental to neurons under conditions of oxidative stress [13–15]. Calcineurin inhibitors, FK506 and SDZ ASM 981, were shown to be neuroprotective in the rat model of transient middle cerebral artery occlusion [16].

Hypoxic-ischemic encephalopathy (HIE) due to perinatal asphyxia (impaired respiratory gas exchange accompanied by acidosis) is a major cause of neurological disability in term neonates with the incidence of 1–8 per 1000 live births in developed countries and as high as 26 per 1000 live births in underdeveloped countries [17], causing as many as a million annual deaths worldwide [18]. Neonatal HIE has heterogeneous causes, and antepartum factors such as pre-eclampsia, maternal thyroid disease, and intrauterine growth retardation, as well as acute intrapartum obstetrical events, have been associated with this condition [19]. The implications of neonatal HIE include mental retardation, cerebral palsy, epilepsy and seizure disorders, motor impairments, and visual and auditory impairments [20, 21]. Despite the recent advances in clinical and basic experimental research, the clinical prognosis for HIE remains poor suggesting that there is a need for novel therapies [19].

Using a mouse neonatal model of HIE, we demonstrated in the present study the involvement of TRPM7 in cell death via p38 and actin modulation through upstream calcium-dependent calcineurin. Here, we employed a combination of pharmacological, proteomic, and biochemistry approaches. To identify the involvement of TRPM7, we used a potent and selective TRPM7 antagonist, waixenicin A, which is a secondary metabolite of the Hawaiian soft coral *Sarcothelia edmondsoni* [22]. A goal of this study was to test the hypothesis that waixenicin A provides neuroprotection in neonatal hypoxic-ischemic model in mice. Additionally, this study aimed to identify some of the key downstream proteins involved in TRPM7 signaling under ischemic conditions in the brain and to validate a pharmacological tool for potential drug development. Using a variety of histological and neurobehavioral assessments in a mouse model of neonatal HIE, we showed that waixenicin A treatment before and up to 1 h after the induction of hypoxia-ischemia reduces brain injury and improves short-term and long-term functional recovery.

Materials and Methods

Experimental Design and Statistical Analysis

The assessment of the neuroprotective effects of the compound was performed on CD1 postnatal day 7–35 mouse pups with histology, immunohistochemistry, and neurobehavioral testing. Experimenters were blinded during drug administrations, neurobehavioral assessments, and histological assessments. Mouse pups were randomly assigned to different treatments and both male and female pups were used in all of the experiments. The effects of the compounds of TRPM7-like current and Ca^{2+} dynamics were performed on CD1 embryonic day 16 neuronal cultures and TRPM7 overexpressed HEK-293 cell line. Sample size (N) for each experiment is indicated in the figure legends corresponding to the experiment. Power analysis was used to determine the number of the animal uses. In brief, using the SigmaPlot software version 11 (Jandel Scientific), based on pilot studies, approximately $n = 8$ per group provided a power of 0.95 to discern a 95% difference between controls and drug-treated animals at alpha = 0.05 [23]. Considering around 80–90% successful rate for the HI in the P7 mouse pups, the final sample size for assessing brain damage in the HI will be at least ~10 pups per testing group (8/0.8 = 10, by adding 20% more pups in the final estimate). All data are presented as mean ± SEM. Statistical differences were analyzed using one-way ANOVA with Bonferroni post hoc for multiple groups or a Student t test for two-group comparisons. $p < 0.05$ was taken as statistically significant.

Animals

All procedures were performed in accordance with animal welfare guidelines at the University of Toronto and were approved by the institutional animal care and use committee. Timed pregnant CD1 mice were obtained from Charles River laboratories (Sherbrooke, Quebec, Canada) and housed at an ambient temperature of 20 ± 1 °C and a 12-h light/dark cycle with food and water fed ad libitum. Postnatal day 7 (P7) pups were used in all experiments. All procedures and protocols were carried out in accordance with Canadian Council on Animal Care guidelines and approved by University of Toronto Animal Care Committee.

Drug Administration

Waixenicin A was extracted and isolated from freeze-dried *Sarcothelia edmondsoni* as previously described [22], aliquoted in single use quantities, and stored at -20°C under desiccant. Prior to use, the compound wasdissolved in methanol and diluted in saline. P7 pups of either sex were randomly assigned to either vehicle or waixenicin A groups. The compound was administered by intraperitoneal injection as a single dose of 37 ng/g body weight in 100 μl of saline solution with 0.0037% methanol. For vehicle controls, an equal volume of vehicle solution (saline with 0.0037% methanol) was administered in an identical manner. The treatment timelines are illustrated in Fig. 1 a, as well as explained below:

Pre-treatment or pre-ischemia: waixenicin A or vehicle solution was administered 30 min prior to surgical occlusion of common carotid artery.

Post-treatment 1 or post-ischemia: waixenicin A or vehicle solution was administered 30 min prior to onset of hypoxia.

Post-treatment 2 or immediately post-hypoxia: waixenicin A or vehicle solution was administered immediately after hypoxic treatment.

Post-treatment 3 or 1 h post-hypoxia: waixenicin A or vehicle solution was administered 1 h after hypoxic treatment.

Naltriben mesylate (Tocris, no. 0892) was administered before ischemia by intraperitoneal injection as a single dose of 42 μg/g of body weight in 100 μl of saline solution (0.004% DMSO). For vehicle controls, an equal volume of saline (0.004% DMSO) was administered in an identical manner.

Neonatal Hypoxic-Ischemic Brain Injury Model

A modified method of Rice-Vannucci procedure [24] of neonatal hypoxic-ischemic (HI) brain injury was carried out as described previously [25, 26]. Briefly, P7 pups of either sex weighting 5–5.5 g were anesthetized with isoflurane (3.0% for induction and 1.5% for maintenance). Body temperature of the pups was monitored and maintained in the heat pad (~ 37 °C) throughout all the procedures. The right common carotid artery (CCA) was exposed and ligated using bipolar electrical coagulation (Vetroson). The incision was closed with tissue adhesive (3M Vetbond). Mice were then returned to their dam with heat pad (~ 37 °C) and allowed to recover for 90 min. Subsequently, pups were placed in an airtight, transparent chamber (A-Chamber A-15274 with ProOx 110 Oxygen Controller/E-720 Sensor, Biospherix, NY, USA) perfused with humidified gas mixture containing 7.5% oxygen balanced with 92.5% nitrogen at 37 °C for 60 min. After the hypoxia procedure, the pups were placed on a heat pad (~ 37 °C) and monitored for 15–20 min until fully awake then returned to the dam afterwards. Chamber temperature was monitored using a homoeothermic blanket control unit (K-017484 Harvard Apparatus, MA, USA). Sham controls were subjected to anesthesia and the common carotid artery was exposed without ligation and subsequent exposure to hypoxia.

Infarct Volume and Histological Assessments

Twenty-four hours after HI injury, whole brains were removed from P8 pups and sectioned coronally into approximately 1-mm slices. Slices were stained with 1% 2,3,5-triphenyl-2H-tetrazolium chloride (TTC) in saline and placed in a dark incubator maintained at 37 °C for 20 min. The corrected infarct volumes were calculated as follows: corrected infarct volume (%) = ((contralateral hemisphere volume – ipsilateral hemisphere + infarct volume)/contralateral hemisphere volume) × 100%, as described previously [25, 26]. Seven days after HI injury, whole brains were removed, fixed, imaged, sectioned coronally into approximately 100-μm slices, and stained with Nissl (0.1% cresyl violet), as described previously [25, 26]. Thirty-two days after HI injury, whole brains were removed, fixed, and imaged, and hemispheric liquefaction volumes were calculated. The hemispheric liquefaction volumes and infarct volumes were measured using the ImageJ software (National institute of Health, Bethesda, MD, USA), as described previously [25, 26].

Neurobehavioral Assessments

Pups in all treatment groups were subjected to the following highly reproducible strain- and gender-independent neurobehavioral assessments 1, 3, and 7 days after HI, as described previously [25, 26]. To evaluate the effects of waixenicin A on functional recovery after HI injury, all behavior tests were carried out following HI focus on brain damage–associated sensorimotor dysfunctions in different developmental stages to assess vestibular, proprioceptive, and motor functions as well as strength and fatigability of muscles [27, 28]. All short- and long-term behavioral tests exhibited are not sex and strain specific [25]. Those behavioral tests include the following: (1) *righting reflex*, where animals were placed in supine position and the time needed to get to prone position is

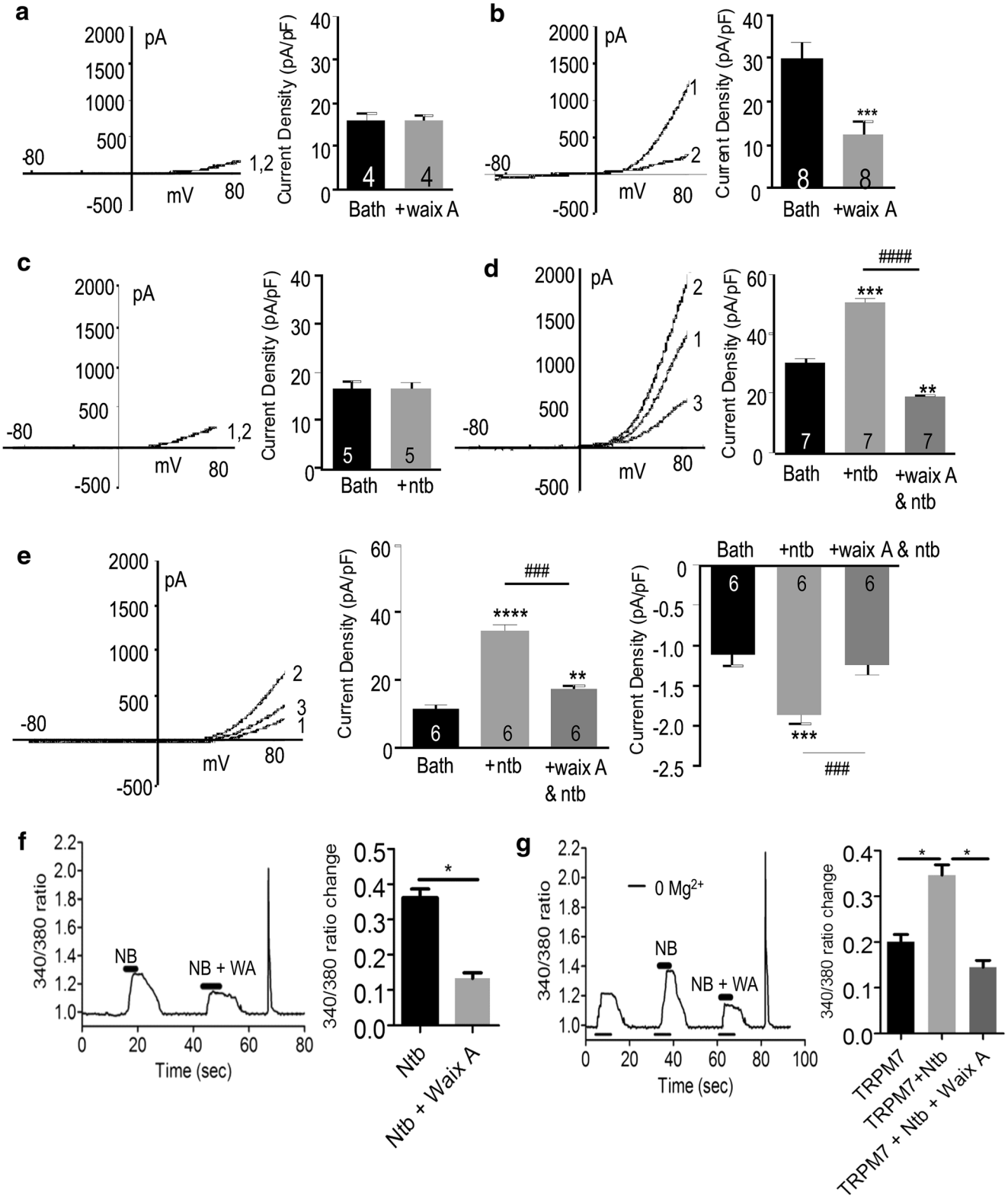

recorded; (2) *cliff avoidance reflex*, where animals were placed with forepaws over the edge and the time required to turn at least 90° was recorded; (3) *geotaxis reflex*, where animals were placed on an inclined board (45°) facing downwards and the time required to turn around is recorded; (4) *grip strength test*, where animals were allowed to hang on a horizontal wire by forelimbs and the time to release the wire was recorded.

◀ **Fig. 1** Effects of waixenicin A and naltriben on TRPM7-like currents in TRPM7-overexpressing tetracycline-inducible HEK293 cells and dissociated hippocampal neurons. (**a**) Representative current-voltage (IV) trace of TRPM7 current (1 = bath; 2 = waixenicin A and TRPM7 outward current in non-induced HEK293 cells ($p > 0.05$; $n = 4$). (**b**) Representative IV trace of TRPM7 current (1 = bath; 2 = waixenicin A) and TRPM7 outward current in TRPM7-overexpressed HEK293 cells ($p < 0.001$; $n = 8$). (**c**) Representative IV trace of TRPM7 current (1 = bath; 2 = naltriben) and TRPM7 outward current in non-induced HEK293 cells ($p > 0.05$; $n = 5$). (**d**) Representative IV trace of TRPM7 current (1 = bath; 2 = naltriben; 3 = waixenicin A + naltriben) and outward current in TRPM7-overexpressed HEK293 cells (**$p < 0.01$; ***$p < 0.001$; ####$p < 0.0001$ ($n = 7$)). (**e**) Representative IV trace of TRPM7 current (1 = bath; 2 = naltriben; 3 = waixenicin A + naltriben) and TRPM7 outward (left) and inward (right) currents in primary hippocampal neurons (**$p < 0.01$; ***/###$p < 0.001$; ****$p < 0.0001$ ($n = 6$)). (**f**) Representative 340/380 fura-2 ratio trace recorded from DIV4 hippocampal neurons and TRPM7 calcium influx under basal conditions (in mM: 140 NaCl, 10 HEPES, 4 KCl, 2 $CaCl_2$, 1 $MgCl_2$, 10 glucose) (*$p < 0.05$, $n = 34$). (**g**) Representative 340/380 fura-2 ratio trace recorded from DIV4 hippocampal neurons and TRPM7 calcium influx under low-calcium and magnesium-free conditions (in mM: 140 NaCl, 10 HEPES, 4 KCl, 0.5 $CaCl_2$, 0 $MgCl_2$, 10 glucose) (*$p < 0.05$, $n = 19$). All data presented as mean ± SEM. Statistical analysis was done by Student *t* test or one-way ANOVA with Bonferroni post hoc (*$p < 0.05$)

Accelerated Rotarod Test

Four weeks after the HI procedure, mice in all three groups underwent the accelerated rotarod test (LE8205, Panlab, Harvard Apparatus, Barcelona, Spain) to test for balance and motor function. The speed rotation of the drum accelerated from 4 to 40 rpm within 120 s, and the latency and velocity at which each mouse fell off the drum were recorded. The test was repeated for three consecutive trials and the results were averaged.

Passive Avoidance Test

Four weeks after the HI procedure, mice in all three groups underwent the passive avoidance test to test for the ability to inhibit innate preference for a dark confined space after a single association with an aversive stimulus [29], as described previously [30]. The training protocol consisted of three sessions performed on separate days: habituation, acquisition, and retention. The apparatus consisted of a large (250 (*W*) × 250 (*D*) × 240 (*H*) mm), illuminated compartment and a small (195 (*W*) × 108 (*D*) × 120 (*H*) mm), dark compartment with an electrified grid floor separated by a guillotine gate (LE872, Panlab, Harvard Apparatus, Barcelona, Spain). During habituation session, the mouse was placed into the illuminated compartment and allowed to explore for 1 min. After 1 min, the door to the dark compartment was opened, latency to enter the dark room was recorded (step-through maximal latency: 300 s), and the door was closed for 30 s before the mouse was returned to its home cage. During acquisition session, the protocol was the same as habituation session, but the mouse received an inescapable foot shock (0.4 mA, 2 s) upon entering the dark compartment. The retention session took place 48 h after acquisition session. The mouse was placed into the illuminated compartment, the door to the dark compartment was opened after 5 s, and latency to enter the dark compartment was recorded (step-through maximal latency: 300 s). The latency to enter the dark compartment during the retention session was taken as an index of memory performance.

Novel Object Recognition

Four weeks after HI procedure, the mice in all three groups underwent novel object recognition test to evaluate spontaneous exploratory behavior triggered by novelty [31], as described previously [32]. The objects used for this test were similar in size and odor, but different in shape and texture. The test was carried out in two sessions separated by an intersession interval of 4 h [33]. During familiarization session, the mouse was placed in an open-field arena (25 cm × 25 cm × 24 cm) facing away from two identical objects placed 5 cm apart, and was allowed to explore both objects freely for 3 min of session duration [32]. During the test session, one of the familiar objects was replaced by an identical copy to avoid olfactory cues [32], and another familiar object was replaced by a novel object. The mouse was placed in an open-field arena facing away from the objects and allowed to explore the objects freely for 3 min of session duration. The exploration time of each object was recorded and preference for novel object was calculated as a percentage of total exploration time.

Immunohistochemistry and Confocal Imaging

Brains were collected from pups in all treatment groups 3 days after HI at P10 and fixed in 4% paraformaldehyde/30% sucrose in PBS solution at 4 °C overnight. Brains were embedded into cryomatrix embedding resin (no. 6769006, Thermo Fisher Scientific, Ottawa, ON, Canada), sectioned coronally into 80-μm slices with Leica CM3050 S cryostat (Leica, Concord, ON, Canada). Slices were then washed with 1× PBS for 15 min and probed with mouse anti-NeuN antibody (MAB377, 1:200, Chemicon, CA, USA), rat anti-GFAP (ab7260, 1:1000, Abcam, USA), rabbit anti-caspase-3 (no. 9661, 1:500, Cell Signaling Technology, MA, USA), and mouse anti-TRPM7 (ab85016, 1:500, Abcam, USA) at 4 °C overnight. Subsequently, slices were washed in 1× PBS and probed with secondary goat anti-mouse IgG Alexa Fluor 488 conjugate (A11001, Thermo Fisher Scientific, Ottawa, ON, Canada), goat anti-rat IgG Alexa Fluor 568 conjugate (A11077, Thermo Fisher Scientific, Ottawa, ON, Canada), or goat anti-rabbit IgG Alexa Fluor 405 conjugate (A31556, Thermo Fisher Scientific, Ottawa, ON, Canada) for 1 h at room temperature, washed with 1× PBS and mounted on glass

coverslips with ProLong Gold antifade reagent (P36930, Thermo Fisher Scientific, Ottawa, ON, Canada). Slices were imaged with a Zeiss LSM 700 confocal laser scanning microscope (Zeiss, Germany). Three coronal slices per brain and 3–6 brains per treatment group were used. Quantitative analysis was performed by counting cells in 5–7 random fields with × 20 objective in the ipsilateral (penumbra) and contralateral hemispheres, as previously described [25, 34].

Cell Culture

TRPM7-overexpressing tetracycline-inducible HEK-293 cells were cultured as described previously [35]. Briefly, HEK-293 cells with stable expression of Flag-murine TRPM7/pCDNA4 were cultured with MEM supplemented with 10% FBS, blasticidin (5 μg/ml, Sigma-Aldrich, USA), Glutamax-1 (2 mM, Invitrogen, USA), and zeocin (0.4 mg/ml, Invitrogen, USA). TRPM7 expression was induced by adding 1 μg/ml tetracycline (Sigma-Aldrich, USA) to the culture.

Embryonic primary hippocampal neurons were cultured from E16 CD1 mice as described previously [36]. Briefly, dissected hippocampi were digested with 0.025% trypsin/EDTA at 37 °C for 15 min. Cell density was determined using an improved Neubauer hemocytometer, and 1.0×10^4 cells were plated on poly-D-lysine–coated glass coverslips (Sigma) (12 mm no. 1 German Glass, Bellco cat. no. 1943-10012). The cells were kept in 5% CO_2 at 37 °C in a serum-free culture medium (neurobasal medium supplemented with 1.8% B-27, 0.25% Glutamax, and 1% antibiotic-antimycotic).

Electrophysiological Recordings

Whole-cell TRPM7-like currents were recorded from DIV3 to DIV7 cultured mouse hippocampal neurons and non-induced and induced HEK-293 cells as described previously [36], using an Axopatch 700B (Axon Instruments, Inc.). Currents were recorded using a 400-ms voltage ramp protocol (− 100 to + 100 mV) with an interval of 5 s at 2 kHz and digitized at 5 kHz. pClamp 9.2 software was used for data acquisition and Clampfit 9.2 was used for data analysis. All experiments were carried out at room temperature. Patch pipette resistance was between 5 and 9 MΩ after filling with pipette solution containing (in mM): 145 cesium methanesulfonate, 8 NaCl, 10 EGTA, and 10 HEPES, pH adjusted to 7.2 with CsOH. The bath solution contained (in mM) 140 NaCl, 5 KCl, 2 $CaCl_2$, 20 HEPES, and 10 glucose (pH adjusted to 7.4 with NaOH). The cells were perfused with 500 nM waixenicin A (Hawaii Pacific University) or 50 μM naltriben mesylate (Tocris, cat no. 0892).

Fura-2 Ratiometric Ca^{2+} Imaging

Intracellular Ca^{2+}concentration was measured using a Fura-2 ratiometric Ca^{2+} imaging system as described previously [36]. Neurons were pre-loaded with Fura-2 AM (2 μM) in the dark for 30 min at room temperature, which was then washed with normal physiological solution. Fura-2 Ca^{2+} signal (510-nm emission) was acquired at alternate excitation wavelengths of 340 and 380 nm by a Deltaram V single monochromator controlled by EasyRatioPro (PTI), while neurons were perfused with basal solution containing (mM) 129 NaCl, 2 $CaCl_2$, 1 $MgCl_2$, 25 HEPES, 30 glucose, and 5 KCl (with pH of 7.3–7.4 and osmolality ranging from 320 to 330 mOsm), or low Mg^{2+}/Ca^{2+} solution (0 $MgCl_2$, 0.5 $CaCl_2$) with or without 500 nM waixenicin A, 50 μM naltriben, or both. To avoid phototoxicity and bleaching, exposure of cells to UV light was limited to under 10 s, and the intensity of the excitation light is bypassed through a neutral density filter. Signals were digitized by an intensified charged-coupled device (ICCD) camera (PTI), and fluorescence intensity (Poenie-Tsien) ratios of images were calculated by using EasyRatioPro.

Proteomic Analysis

Proteomic analysis was performed by Proteomics, Analytics, Robotics & Chemical Biology Centre at The Hospital for Sick Children.

TMT Q-Exactive Sample Preparation and Analysis

Samples were reduced, alkylated, digested, and TMT labeled according to manufacturer's directions (Thermo Fisher TMT 10 Plex, Product 90110). Labeled peptides from all samples were combined and lyophilized. Peptides were then fractionated into 3 fractions using the Pierce High pH Reversed-Phase Peptide Fractionation Kit (Pierce Cat 84868) as per manufacturer's directions (fractions 3, 5, *X*). Samples were analyzed on a Orbitrap analyzer (Q-Exactive, Thermo Fisher, San Jose, CA) outfitted with a nanospray source and EASY-nLC nano-LC system (Thermo Fisher, San Jose, CA). Lyophilized peptide mixtures were dissolved in 0.1% formic acid and loaded onto a 75 μm × 50 cm PepMax RSLC EASY-Spray column filled with 2 μM C18 beads (Thermo Fisher, San Jose, CA) at a pressure of 800 bar and a temperature of 60 °C. Peptides were eluted over 180 min at a rate of 250 nl/min using a gradient setup as 0–40% gradient of buffer A (0.1% formic acid; and buffer B, 0.1% formic acid in 80% acetonitrile). Peptides were introduced by nano-electrospray into the Q-Exactive mass spectrometer (Thermo Fisher). The instrument method consisted of one MS full scan (525–1800 m/z) in the Orbitrap mass

analyzer with an automatic gain control (AGC) target of 5e5, maximum ion injection time of 100 ms, and a resolution of 35,000 followed by 15 data-dependent MS/MS scans with a resolution of 35,000, an AGC target of 5e5, maximum ion time of 100 ms, and one microscan. The intensity threshold to trigger a MS/MS scan was set to an underfill ratio of 1.0%. Fragmentation occurred in the HCD trap with normalized collision energy set to 28. The dynamic exclusion was applied using a setting of 35 s.

Database Searching

Tandem mass spectra were extracted, and charge state deconvoluted and deisotoped by Xcalibur version 2.2. All MS/MS samples were analyzed using Sequest (Thermo Fisher Scientific, San Jose, CA, USA; version 1.4.1.14) and X! Tandem (The GPM, thegpm.org; version CYCLONE (2010.12.01.1)). Both search engines were set up to search Uniprot-Mus Musculus-Oct-172016_reviewed.fasta (Download Oct 172016, 16818 entries) assuming the digestion enzyme trypsin. Sequest and X! Tandem were searched with a fragment ion mass tolerance of 0.020 Da and a parent ion tolerance of 20 PPM. Carbamidomethyl of cysteine and TMT6plex of lysine and the n-terminus were specified in Sequest and X! Tandem as fixed modifications. Deamidation of asparagine and glutamine and oxidation of methionine were specified in Sequest as variable modifications. Glu->pyro-Glu of the n-terminus, ammonia-loss of the n-terminus, gln->pyro-Glu of the n-terminus, deamidation of asparagine and glutamine, and oxidation of methionine were specified in X! Tandem as variable modifications.

Criteria for Protein Identification

Scaffold (version Scaffold_4.8.4, Proteome Software Inc., Portland, OR) was used to validate MS/MS-based peptide and protein identifications. Peptide identifications were accepted if they could be established at greater than 95.0% probability by the Scaffold Local FDR algorithm. Protein identifications were accepted if they could be established at greater than 95.0% probability and contained at least 2 identified peptides. Protein probabilities were assigned by the Protein Prophet algorithm [37]. Proteins that contained similar peptides and could not be differentiated based on MS/MS analysis alone were grouped to satisfy the principles of parsimony. Proteins were annotated with GO terms from GOA mouse.gaf (downloaded Nov 11, 2016) [38].

Quantitative Data Analysis

Scaffold Q+ (version Scaffold_4.8.4, Proteome Software Inc., Portland, OR) was used to quantitate label-based quantitation (iTRAQ, TMT, SILAC, etc.) and peptide and protein identifications. Peptide identifications were accepted if they could be established at greater than 95.0% probability by the Scaffold Local FDR algorithm. Protein identifications were accepted if they could be established at greater than 95.0% probability and contained at least 2 identified peptides. Protein probabilities were assigned by the Protein Prophet algorithm [37]. Proteins that contained similar peptides and could not be differentiated based on MS/MS analysis alone were grouped to satisfy the principles of parsimony. Normalization was performed iteratively (across samples and spectra) on intensities, as described in "Statistical Analysis of Relative Labeled Mass Spectrometry Data from Complex Samples Using ANOVA" [39]. Means were used for averaging. Spectral data were log-transformed, pruned of those matched to multiple proteins and those missing a reference value, and weighted by an adaptive intensity weighting algorithm. Of 207,066 spectra in the experiment at the given thresholds, 189,703 (92%) were included in quantitation.

Protein network analysis was performed using STRING 10.5 (https://string-db.org/). Heatmap of the proteins was created using the heatmap3 package in RStudio.

Western Blotting

Western blotting was performed as described previously [4, 25, 34]. Pups were sacrificed and brain samples were collected on dry ice 24 h after HI. Proteins of the ipsilateral hemisphere were extracted in RIPA buffer (Santa Cruz Biotechnology, sc-24948) with protease inhibitor mixture (Santa Cruz Biotechnology, sc-29131). Protein concentrations were determined using the bicinchoninic acid (BCA) method (Pierce). The protein samples (20 μg/well) were separated on a 10% SDS-PAGE gel and proteins were then transferred to a nitrocellulose membrane (200 mA per gel, 60 min). Membranes were incubated with specific primary antibodies against α-actinin-1 (1:2000; ab18061), CaMKII (1:1000; sc-5306), p-CaMKII (1:3000; sc-12886), calcineurin B (1:3000; ab154650), calmodulin (1:2000; ab107977), p38 (1:1000; 9212S), p-p38 (1:2000; 4511S), cleaved caspase 3 (1:1000; Cell Signaling 9664), cleaved caspase 9 (1:1000; Cell Signaling 9504S), Bax (1:1000; Cell Signaling 2772), Bcl-2 (1:1000; Cell Signaling 2870), p-cofilin (1:2000; ab12866), cofilin (1:3000; ab134963), β-actin (1:3000; Sigma), and GAPDH (1:10,000, 2118S) at 4 °C overnight. Horseradish peroxidase–conjugated anti-mouse (1:7500; Chemicon AP130P), anti-rabbit (1:7500; Chemicon AP132S), and anti-goat (1:7500; Chemicon AP180P) IgG antibodies were used as secondary antibodies and were detected with the ECL system (Perkin Elmer, Inc., USA). Images were analyzed using an image-analysis system (NIH ImageJ 1.47v). Protein expression was normalized to that of β-actin and expressed as part of control.

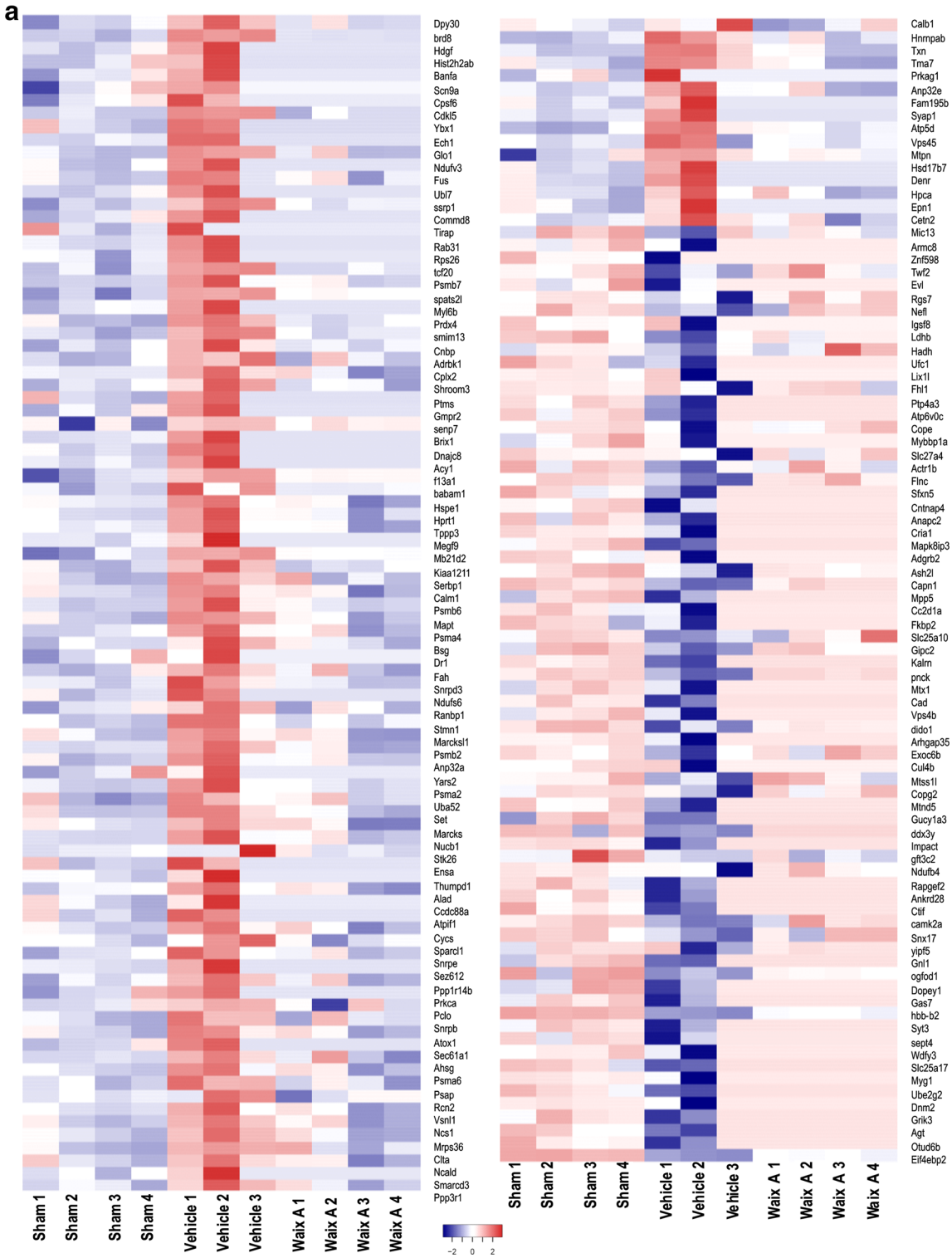

Fig. 2 Proteomic changes 6 h following hypoxic-ischemic brain injury in a pre-treatment paradigm. (**a**) Heatmap showing relative changes (log_2 values of fold change) in expression of 95 proteins between sham, vehicle, and waixenicin A groups, and an interaction network of these proteins generated by STRING 10.5. (**b**) Interaction network and a list of proteins with molecular function of calcium binding. (**c**) Changes in CaMKII ($p = 0.0004$, $n = 4$), calcineurin (regulatory subunit B) ($p = 0.0083$, $n = 4$), and calmodulin ($p = 0.0138$, $n = 4$) levels, as detected by LC-MS/MS 6 h after HI. All data presented as mean ± SEM. Statistical analysis: one-way ANOVA with Bonferroni post hoc, $^*p < 0.05$

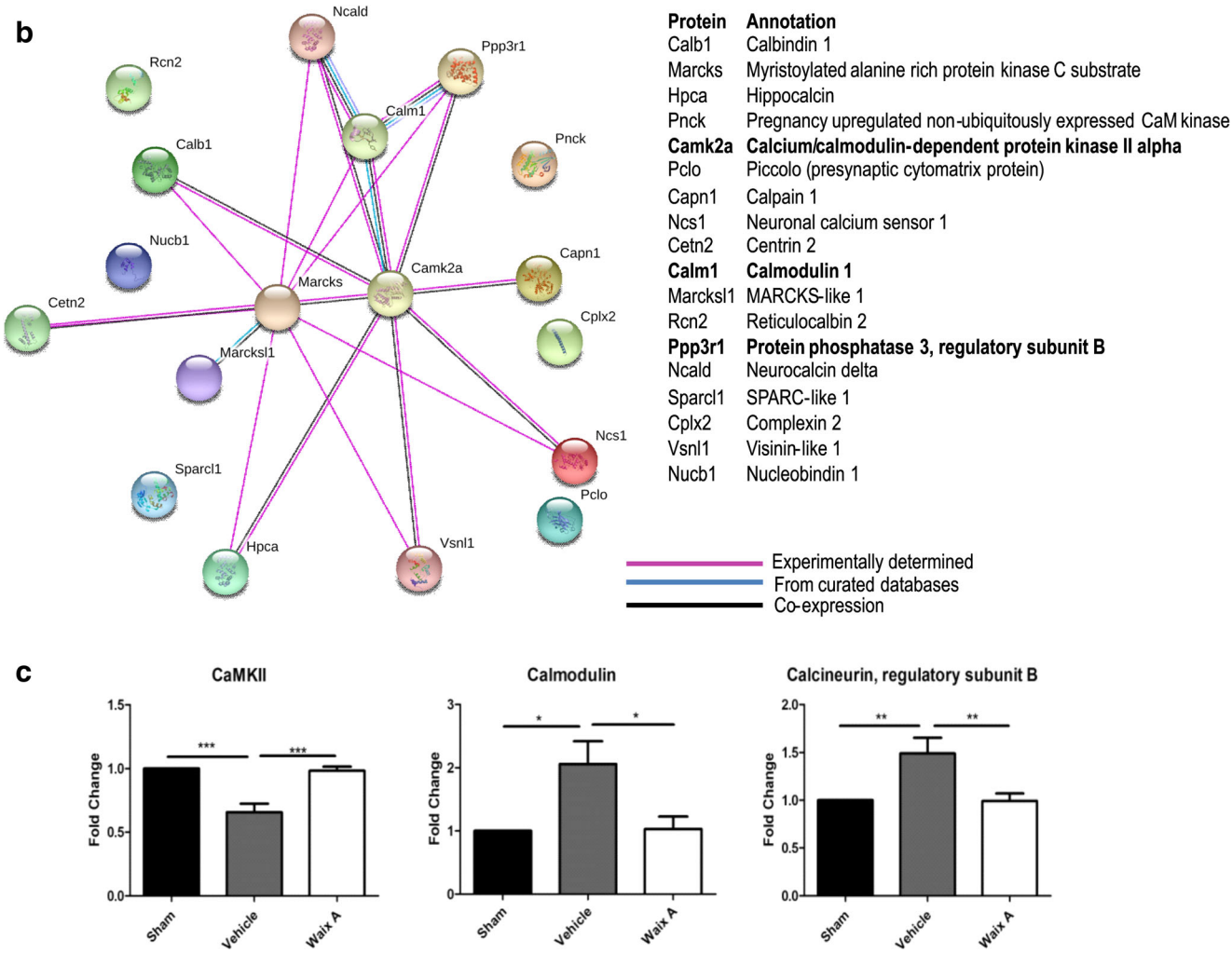

Fig. 2 continued.

Results

Waixenicin A and Naltriben Modulate TRPM7 and TRPM7-Like Currents in TRPM7-Overexpressing HEK-293 Cells and Cultured Hippocampal Neurons

To confirm the inhibitory effect of waixenicin A on TRPM7 current, we first carried out whole-cell patch-clamp recording on HEK293 cells overexpressing recombinant TRPM7 channels. Tetracycline was used to induce TRPM7 overexpression in HEK293 cells. Figure 1 b shows that the TRPM7 currents in HEK293 cells treated with tetracycline were large and outwardly rectifying. The TRPM7 inhibitor, waixenicin A (500 nM), significantly reduced TRPM7 current density at + 100 mV by ~ 60% (from 30 ± 4 pA/pF to 13 ± 3 pA/pF) in the HEK293 cells induced with tetracycline (Fig. 1b). On the contrary, the TRPM7 agonist, naltriben (10 μM), potentiated the TRPM7 current density by ~ 70% (from 31 ± 4 pA/pF to 51 ± 7 pA/pF; Fig. 1d), and was also sensitive to block by waixenicin A (the naltriben-potentiated current was reduced to 19 ± 2 pA/pF; Fig. 1d). In HEK293 cells without induction by tetracycline, neither waixenicin A (Fig. 1a) nor naltriben (Fig. 1c) had any effect on the endogenous current.

We next tested whether naltriben can activate TRPM7-like currents in DIV4-7 primary mouse hippocampal neurons, and if so, whether waixenicin A can reduce this current. As shown in Fig. 1 e (middle), the current density of the basal outwardly rectifying current al + 100 mV was 11 ± 2 pA/pF. Perfusion of naltriben potentiated TRPM7-like currents by threefold, and the current density became 34 ± 2 pA/pF. Subsequent waixenicin A perfusion significantly reduced the naltriben-potentiated current by ~ 50% to 17 ± 1 pA/pF. Additionally, naltriben also potentiated the inward current at − 100 mV by ~ 65% (from − 1.1 ± 0.3 pA/pF to − 1.9 ± 0.4 pA/pF), and subsequently reversed by waixenicin A (to − 1.2 ± 0.3; $p < 0.001$, Fig. 1e (right)).

Our results suggest that TRPM7 channels are functional in primary mouse hippocampal neurons and channel activity is sensitive to inhibition by waixenicin A.

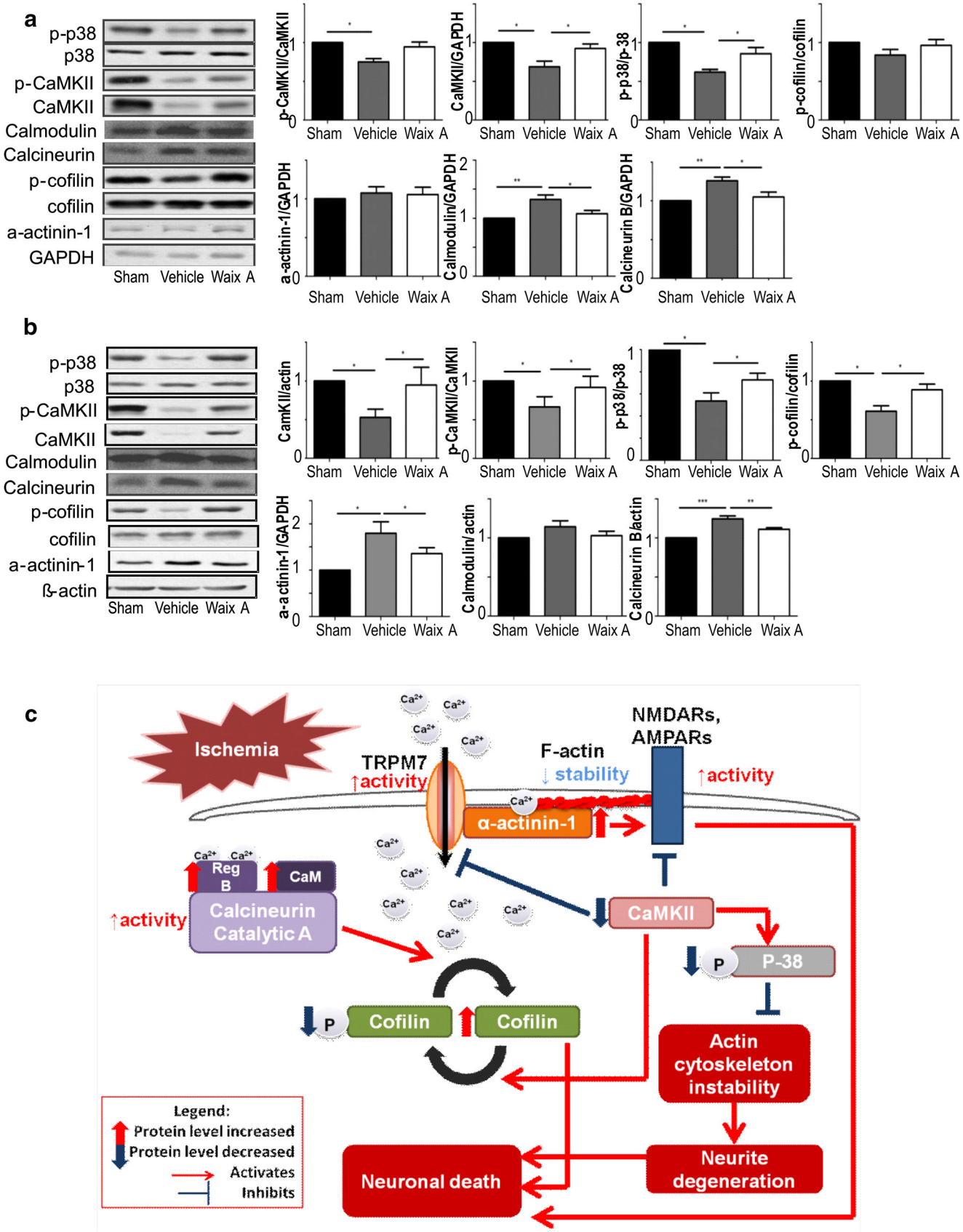
a
p-p38
p38
p-CaMKII
CaMKII
Calmodulin
Calcineurin
p-cofilin
cofilin
a-actinin-1
GAPDH
Sham Vehicle Waix A
p-CaMKII/CaMKII
CaMKII/GAPDH
p-p38/p-38
p-cofilin/cofilin
a-actinin-1/GAPDH
Calmodulin/GAPDH
Calcineurin B/GAPDH
b
p-p38
p38
p-CaMKII
CaMKII
Calmodulin
Calcineurin
p-cofilin
cofilin
a-actinin-1
ß-actin
CamKII/actin
p-Ca MKII/CaMKII
p-p38/p-38
p-cofilin/cofilin
a-actinin-1/GAPDH
Calmodulin/actin
Calcineurin B/actin
c
Ischemia
TRPM7
↑activity
F-actin
↓ stability
NMDARs,
AMPARs
↑activity
α-actinin-1
Reg B
CaM
↑activity
Calcineurin
Catalytic A
CaMKII
P
P-38
P
Cofilin
Cofilin
Actin
cytoskeleton
instability
Neurite
degeneration
Neuronal death
Legend:
Protein level increased
Protein level decreased
Activates
Inhibits

◀ **Fig. 3** Biochemical assessment of signaling pathways affected by hypoxic-ischemic insult on neonatal brain in a pre-treatment paradigm. (**a**) Changes in downstream signaling of CaMKII and calcineurin as detected by Western blot 6 h after HI. Significant changes were detected in CaMKII ($p = 0.0366$), calmodulin ($p = 0.014$), calcineurin B ($p = 0.01$), p-CaMKII/CaMKII ratio ($p = 0.0062$), and p-p38/p38 ratio ($p = 0.0015$). Alpha-actinin-1 levels showed an increasing trend ($p = 0.7456$), while p-cofilin/cofilin ratio showed a decreasing trend ($p = 0.1889$); control group: $n = 4$; vehicle group: $n = 4$; waixenicin A group: $n = 4$. (**b**) Changes in downstream signaling of CaMKII and calcineurin as detected by Western blot 24 h after HI. Significant changes were detected in CaMKII ($p = 0.0378$), calcineurin B ($p < 0.001$), p-CaMKII/CaMKII ($p = 0.0361$), p-p38/p38 ratio ($p < 0.0001$), alpha-actinin-1 levels ($p = 0.001$), and p-cofilin/cofilin ratio ($p = 0.033$); control group: $n = 4$; vehicle group: $n = 4$; waixenicin A group: $n = 4$. Calmodulin levels showed an increasing trend. (**c**) Proposed TRPM7-mediated signaling cascade following HI. The blots were cropped to show representative bands. All data presented as mean ± SEM. Statistical analysis: one-way ANOVA with Bonferroni post hoc, $*p < 0.05$

Waixenicin A and Naltriben Modulate TRPM7 Ca^{2+} Dynamics in Primary Hippocampal Neurons

To determine the effect of waixenicin A and naltriben on TRPM7 Ca^{2+} dynamics, we performed fura-2 ratiometric Ca^{2+} imaging on DIV4–5 mouse hippocampal neurons. In the basal solution, the perfusion of neurons with 50 μM naltriben resulted in increase of the ratio of emission signal at 510 nm following excitation at 340 nm/380 nm (340/380 ratio) by 0.4 ± 0.02 (Fig. 1f) from the baseline level while subsequent perfusion of naltriben together with 500 nM waixenicin A increased the ratio by a lesser degree of 0.1 ± 0.02 (Fig. 1f) from the baseline level, a 63% reduction in naltriben-induced calcium signal. A representative 340/380 ratio trace for this experiment is shown in Fig. 1 f (left).

Lowering extracellular divalent cation concentrations mimics the "Ca^{2+} paradox" conditions that lead to delayed neuronal death after ischemia [40] and cause an increase in TRPM7 Ca^{2+} influx [4, 36]. Thus, we investigated next the effect of naltriben and waixenicin A on Mg^{2+}-free TRPM7 current in mouse hippocampal neurons. We found that perfusing neurons with Mg^{2+}-free solution increased the net Ca^{2+} signal by 0.2 ± 0.02 from the basal level (Fig. 1g). Perfusion of 50 μM naltriben in Mg^{2+}-free solution resulted in the net increase in Ca^{2+} signal by 0.4 ± 0.02 (Fig. 1g), a 72% increase from Mg^{2+}-free calcium influx. Perfusion of 50 μM naltriben together with 500 nM waixenicin A under Mg^{2+}-free conditions resulted in a smaller increase in Ca^{2+} signal by 0.14 ± 0.01 (Fig. 1g), a 58% reduction in naltriben-induced Ca^{2+} signal and a 28% reduction in Mg^{2+}-free Ca^{2+} influx. These waixenicin A findings were consistent with our previously published data [36]. A representative 340/380 ratio trace for this experiment is shown in Fig. 1 g (left).

These data confirm that naltriben and waixenicin A modulate TRPM7-mediated Ca^{2+} signal in hippocampal neurons under basal and Mg^{2+}-free conditions.

Waixenicin A Attenuates Proteomic Changes Caused by HI 6 h After Injury

Samples from sham, vehicle-treated, and waixenicin A-treated groups were collected 6 h after HI and subjected to liquid chromatography tandem-mass spectrometry (LC-MS/MS) using Orbitrap analyzer. We found 95 proteins that were differentially expressed, displaying more than 1.5-fold change, between sham and vehicle groups and were also identified in waixenicin A group (Fig. 2a, left). The full list of the proteins with Uniprot ID and fold change can be found in Supplementary Table 1. The proteins were uploaded into the STRING 10.5 database [41] to identify protein interactions based on co-expression, information from curated databases, experimentally determined interactions, and text mining (Fig. 2a, right). Since TRPM7 is a calcium-conducting ion channel, we focused on the proteins with molecular function of calcium binding (Fig. 2b). We found that protein levels of Ca^{2+}/calmodulin-dependent protein kinase II (CaMKII) (Uniprot ID P11798), calcineurin (regulatory subunit B) (Uniprot ID Q63810), and calmodulin (Uniprot ID P0DP2) were significantly different between the treatment groups (Fig. 2c, fold change normalized to sham group expression: CaMKII, vehicle-treated group: 0.66 ± 0.07 ($n = 4$), waixenicin A-treated group: 1.00 ± 0.03 ($n = 4$), $p = 0.0004$; calcineurin regulatory subunit B, vehicle-treated group: 1.5 ± 0.3 ($n = 4$), waixenicin A-treated group: 0.99 ± 0.15 ($n = 4$), $p = 0.0083$; calmodulin, vehicle-treated group: 2.06 ± 0.34 ($n = 4$), waixenicin A-treated group: 1.03 ± 0.2 ($n = 4$), $p = 0.0138$).

These data indicate that waixenicin A attenuates HI brain injury potentially through calcium-dependent signaling cascade.

Waixenicin A May Reduce HI Brain Damage Through CamKII, Calmodulin, Calcineurin, and Downstream p38, Cofilin, and α-Actinin-1 Signaling

Next, we examined the changes in CaMKII, calmodulin, and calcineurin levels as well as downstream proteins in sham, vehicle-treated, and waixenicin A-treated groups 6 and 24 h after HI. We found that HI injury significantly reduced CaMKII protein levels and CaMKII and p38 phosphorylation levels, and increased calcineurin B protein levels in the ipsilateral hemisphere, and waixenicin A pre-treatment restored the protein levels of these proteins 6 (Fig. 3a) and 24 h (Fig. 3b) after HI (Fig. 3a: p-p38/p38 normalized to sham group expression: vehicle-treated: 0.62 ± 0.03 ($n = 4$), waixenicin A-treated: 0.86 ± 0.08 ($n = 4$), $p = 0.0015$; CaMKII/β-actin normalized to sham group expression: vehicle-treated: 0.69 ± 0.07 ($n = 4$), waixenicin A-treated: 0.92 ± 0.06 ($n = 4$), $p = 0.0366$; p-CaMKII/CaMKII normalized to sham group expression: vehicle-treated: 0.75 ± 0.04 ($n = 4$); waixenicin A-treated: 0.94 ± 0.06 ($n = 4$), $p = 0.0062$; calcineurin

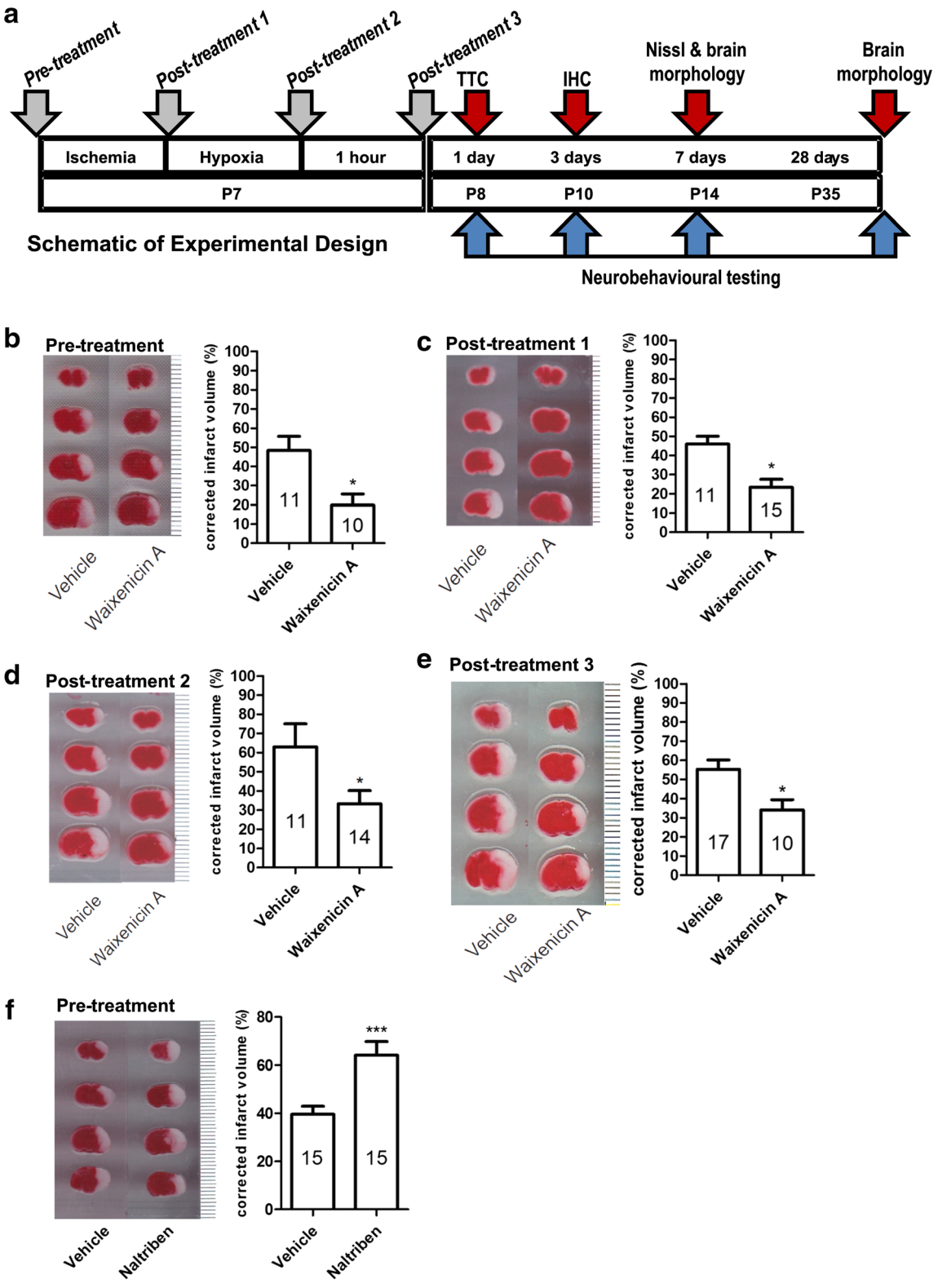

B normalized to sham group expression: vehicle-treated: 1.26 ± 0.05 ($n = 4$); waixenicin A-treated: 1.05 ± 0.06 ($n = 4$), $p = 0.01$; Fig. 3b: p-p38/p38 normalized to sham group expression: vehicle-treated: 0.5 ± 0.07 ($n = 4$); waixenicin A-treated: 0.7 ± 0.06 ($n = 4$), $p < 0.0001$; CaMKII/β-actin normalized to sham group expression: vehicle-treated: 0.53 ± 0.11 ($n = 4$), waixenicin A-treated: 0.95 ± 0.23 ($n = 4$), $p = 0.0378$; p-CaMKII/CaMKII normalized to sham group expression: vehicle-treated: 0.7 ± 0.13

◀ **Fig. 4** Morphological assessment of brain injury 24 h after hypoxic-ischemic insult on neonatal brain. (**a**) Schematic of experimental design detailing the time course of treatment administration and morphological, histological, and behavioral assessments. (**b**) Representative TTC staining and corrected infarct volume of vehicle (48 ± 7, $n = 11$) and waixenicin A (20 ± 6, $n = 10$) groups treated according to pre-treatment paradigm, $p = 0.0077$. (**c**) Representative TTC staining and corrected infarct volume of vehicle (46 ± 4, $n = 11$) and waixenicin A (23 ± 4, $n = 15$) groups treated according to post-treatment 1 paradigm, $p = 0.0028$. (**d**) Representative TTC staining and corrected infarct volume of vehicle (63 ± 12, $n = 11$) and waixenicin A (33 ± 7, $n = 14$) groups treated according to post-treatment 2 paradigm, $p = 0.034$. (**e**) Representative TTC staining and corrected infarct volume of vehicle (55 ± 5, $n = 17$) and waixenicin A (34 ± 5, $n = 10$) groups treated according to post-treatment 3 paradigm, $p = 0.0101$. (**f**) Representative TTC staining and corrected infarct volume of vehicle (40 ± 3, $n = 22$) and naltriben (64 ± 6, $n = 15$) groups treated according to pre-treatment paradigm, $p = 0.0009$. All data presented as mean ± SEM. Statistical analysis was done by Student t test (*$p < 0.05$)

($n = 4$); waixenicin A-treated: 0.9 ± 0.14 ($n = 4$), $p = 0.0361$; calcineurin B normalized to sham group expression: vehicle-treated: 1.24 ± 0.04 ($n = 4$); waixenicin A-treated: 1.11 ± 0.02 ($n = 4$), $p < 0.001$). Calmodulin protein levels were significantly upregulated in the ipsilateral hemisphere in HI group 6 h after injury (Fig. 3a), but not 24 h after injury (Fig. 3b) (Fig. 3a: calmodulin normalized to sham group expression: vehicle-treated: 1.32 ± 0.08 ($n = 4$); waixenicin A-treated: 1.08 ± 0.06 ($n = 4$), $p = 0.014$).

Modification of actin has also been linked to cell death under hypoxic conditions [42–45]. Therefore, we evaluated the effect of HI injury and waixenicin A treatment on the expression levels of two actin-modulating proteins: α-actinin-1 and cofilin. We found that HI injury significantly upregulated α-actinin-1 expression levels and significantly reduced cofilin phosphorylation levels, and waixenicin A pre-treatment restored the levels of these proteins 24 h after HI (Fig. 3b), while there was a similar trend in changes in these proteins 6 h after HI (Fig. 3a) (Fig. 3a: α-actinin-1/β-actin normalized to sham group expression: vehicle-treated: 1.08 ± 0.08 ($n = 4$), waixenicin A-treated: 1.05 ± 0.09 ($n = 4$), $p = 0.7456$; p-cofilin/cofilin normalized to sham group expression: vehicle-treated: 0.84 ± 0.07 ($n = 4$), waixenicin A-treated: 0.96 ± 0.07 ($n = 4$), $p = 0.1889$; Fig. 3b: α-actinin-1/β-actin normalized to sham group expression: vehicle-treated: 1.8 ± 0.24 ($n = 4$), waixenicin A-treated: 1.4 ± 0.13 ($n = 4$), $p = 0.001$; p-cofilin/cofilin normalized to sham group expression: vehicle-treated: 0.6 ± 0.07 ($n = 4$), waixenicin A-treated: 0.9 ± 0.07 ($n = 4$), $p = 0.033$).

These data indicate that waixenicin A acts through several signaling cascades to attenuate the HI brain injury to the neonatal brain (Fig. 3c).

We also assessed the effects of waixenicin A on apoptotic signaling, neuronal survival, and TRPM7 expression by performing biochemical analysis of sham, vehicle-treated, and waixenicin A-treated brains 24 h after HI injury. We found that HI injury upregulated cleaved caspase-3 and caspase-9 levels and significantly reduced Bcl-2/Bax protein ratio, and waixenicin A pre-treatment restored the levels of these proteins (Supplementary Fig. 1A: caspase-9/β-actin normalized to sham group expression: vehicle-treated: 3.6 ± 0.6 ($n = 4$); waixenicin A-treated: 1.2 ± 0.4 ($n = 4$), $p < 0.0001$; caspase-3/β-actin normalized to sham group expression: vehicle-treated: 17 ± 1.2 ($n = 4$); waixenicin A-treated: 8.9 ± 0.8 ($n = 4$), $p < 0.001$; Bcl-2/Bax normalized to sham group expression: vehicle-treated: 0.6 ± 0.02 ($n = 4$); waixenicin A-treated: 1 ± 0.02 ($n = 4$), $p = 0.0279$).

We also performed immunohistochemical staining and analysis of the penumbra area of the brain slices in sham and vehicle- and waixenicin A-treated groups 3 days after HI injury. Representative confocal images are shown in Supplementary Fig. 1B. As seen in Supplementary Fig. 1C, waixenicin A pre-treatment significantly reduced the loss of NeuN-positive cells when compared with the vehicle-treated group (as a part of contralateral hemisphere: sham: 1 ± 0.04; vehicle: 0.5 ± 0.04; waixenicin A: 0.7 ± 0.03). Moreover, we also observed an upregulation of GFAP expression in astrocytes which represents astroglial activation and reactive gliosis during trauma or neurodegeneration in vehicle-treated group which was significantly attenuated in waixenicin A-treated group. These data are shown in Supplementary Fig. 1D and represent GFAP-positive cells per × 20 field (sham: 13 ± 6; vehicle: 245 ± 61; waixenicin A: 41 ± 18). We also found a significant upregulation of cleaved caspase-3 and TRPM7 protein levels in vehicle-treated groups with attenuation of both proteins in the waixenicin A-treated group. This is shown in Supplementary Fig. 1E as the number of cleaved caspase-3-positive cells per × 20 field (sham: 7 ± 1; vehicle: 100 ± 11; waixenicin A: 38 ± 9) and Supplementary Fig. 1F as relative TRPM7 levels compared with contralateral hemisphere (sham 1 ± 0.06; vehicle 2 ± 0.2; waixenicin A 1.3 ± 0.2 of contralateral hemisphere).

These data demonstrate that waixenicin A pre-treatment reduces apoptotic and delayed neuronal cell death and attenuates glial cell activation in ischemic penumbra.

Waixenicin A Reduces Brain Damage When Applied as a Pre-Treatment and up to 1 h After the Onset of the HI Brain Injury

Waixenicin A (37 ng/g) or vehicle (saline with 0.0037% methanol) was administered as a single intraperitoneal injection to postnatal P7 pups according to the timeline in Fig. 4 a. The "pre-treatment" group was injected 30 min before induction of HI. The brains were harvested and stained with triphenyl tetrazolium chloride (TTC) 24 h after injury. We found that compared with the vehicle-treated group, the waixenicin A-treated group had significantly reduced corrected infarct volumes of the ipsilateral

hemispheres (vehicle: 48 ± 7% ($n = 11$); waixenicin A: 20 ± 6%, $n = 10$, $p = 0.0077$), as illustrated in Fig. 4 b (right). Figure 4 b (left) shows representative TTC-stained images of vehicle- and waixenicin A-treated brains 24 h following the injury.

The "post-treatment 1" group received an injection of vehicle or waixenicin A 30 min before the onset of hypoxia. This is to (1) determine if timing of TRPM7 inhibition has any effects, and (2) evaluate whether waixenicin A can confer benefits as a preventative therapeutic strategy to mitigate further hypoxic damage. When compared with the vehicle-treated group, the waixenicin A-treated group also had significantly smaller infarct volumes 24 h following the injury in this treatment paradigm (vehicle: 46 ± 4%, $n = 11$; waixenicin A: 23 ± 4%, $n = 15$, $p = 0.0028$). Figure 4 c (left) shows representative TTC stainings, while Fig. 4 c (right) shows corrected infarct volumes of the ipsilateral hemisphere.

The "post-treatment 2" group received an injection of vehicle or waixenicin A immediately following hypoxia exposure. Figure 4 d (left) shows representative TTC staining, while Fig. 4 d (right) shows a significant reduction in corrected infarct volumes in the waixenicin A-treated group, compared with the vehicle-treated group (vehicle: 63 ± 12%, $n = 11$; waixenicin A: 33 ± 7%, $n = 14$, $p = 0.034$).

The "post-treatment 3" group received an injection of vehicle or waixenicin A 1 h after the hypoxia event. Representative TTC stainings of brains treated with vehicle and waixenicin A are shown in Fig. 4 e (left), while Fig. 4 e (right) shows a significant reduction in corrected infarct volumes in the waixenicin A-treated group compared with the vehicle-treated group (vehicle: 55 ± 5%, $n = 17$; waixenicin A: 34 ± 5%, $n = 10$, $p = 0.0101$) 24 h following the injury.

These data show that application of waixenicin A reduces HI-induced brain damage when administered both before and after HI injury.

Naltriben Exacerbates Brain Damage When Applied as a Pre-Treatment

Next, we examined the effect of TRPM7 activator naltriben [46] on the extent of brain injury following HI induction. Naltriben was injected intraperitoneally as a single dose of 42 μg/g of body weight as a pre-treatment (30 min before the onset of ischemia). The brains were harvested and stained with TTC 24 h following the injury. We found that naltriben application significantly increased the corrected infarct volumes as shown in Fig. 4 f (vehicle (0.001% DMSO): 40 ± 3%, $n = 22$; naltriben: 64 ± 6%, $n = 15$, $p = 0.0009$). These data demonstrate that application of the TRPM7 activator naltriben exacerbates brain damage after neonatal HI.

The purpose of using naltriben in vitro was to demonstrate that waixenicin A is capable of inhibiting enhanced activation of TRPM7, which is important since HI cultivates conditions that promote TRPM7 activity [7]. As described above, we observed in both our patch clamp electrophysiology and Fura-2 Ca^{2+} imaging that waixenicin A treatment (TRPM7 inhibition) overrode naltriben treatment (TRPM7 potentiation). That is, naltriben alone potentiated TRPM7 current and caused a larger Ca^{2+} signal. However, waixenicin A inhibited the TRPM7 current and caused a smaller Ca^{2+} signal, with or without naltriben. From this, we hypothesize that waixenicin A and naltriben are acting on different regions of TRPM7 or working under different mechanisms of action. Regardless, naltriben-mediated effects on TRPM7 are outcompeted by those of waixenicin A. Based on this, we do not speculate that naltriben can rescue neurotoxicity in the presence of waixenicin A treatment in vivo. Further studies can examine these hypotheses.

Waixenicin A Preserves Overall Brain Morphology 7 Days After HI Injury

To determine the effects of waixenicin A treatment on preserving brain morphology following HI injury, we evaluated corrected ipsilateral liquefaction volumes and brain weight in different treatment groups 7 days after HI injury. The overall brain morphology was preserved as shown in Fig. 5 a and b (pre-treatment) and Fig. 5 e and f (post-treatment 2). Waixenicin A-treated groups showed significantly reduced corrected ipsilateral liquefaction volumes as shown in Fig. 5 d (sham: 0, $n = 3$; vehicle: 46 ± 3%, $n = 13$; waixenicin A: 27 ± 3%, $n = 12$, $p < 0.0001$) and Fig. 5 h (sham: 0, $n = 5$; vehicle: 55 ± 6%, $n = 12$; waixenicin A: 34 ± 5%, $n = 11$, $p < 0.0001$) for pre-treatment and post-treatment, respectively. Brain weights were also significantly greater in both waixenicin A pre-treatment and post-treatment groups, as seen in Fig. 5 c (vehicle: 0.28 ± 0.03 g, $n = 14$; waixenicin A: 0.35 ± 0.01 g, $n = 18$, $p = 0.0146$) and Fig. 5 g (vehicle: 0.32 ± 0.01 g, $n = 12$; waixenicin A: 0.38 ± 0.01 g, $n = 11$, $p = 0.0077$), respectively.

These data show that waixenicin A prevents brain mass loss and preserves brain morphology in the short term after HI injury.

Waixenicin A Improves Short-Term Functional Recovery Following HI Injury

To determine the effects of waixenicin A on functional recovery after HI injury, we subjected the pups to multiple tests 1, 3, and 7 days following HI to assess vestibular, proprioceptive, and motor functions as well as strength and fatigability of muscles. We found that both pre-treatment (before ischemia) and post-treatment (immediately after hypoxia) administration of waixenicin A significantly improved outcomes of righting reflex, geotaxis reflex, cliff avoidance reflex, and grip strength test. Righting reflex was significantly improved in waixenicin A-treated group compared with vehicle-treated group 1 day after HI for both paradigms (pre-treatment (Fig. 6a, left) sham: 0.8 ± 0.09 s, $n = 8$; vehicle: 2.7 ± 0.6 s, $n = 13$; waixenicin A: 1.5 ±

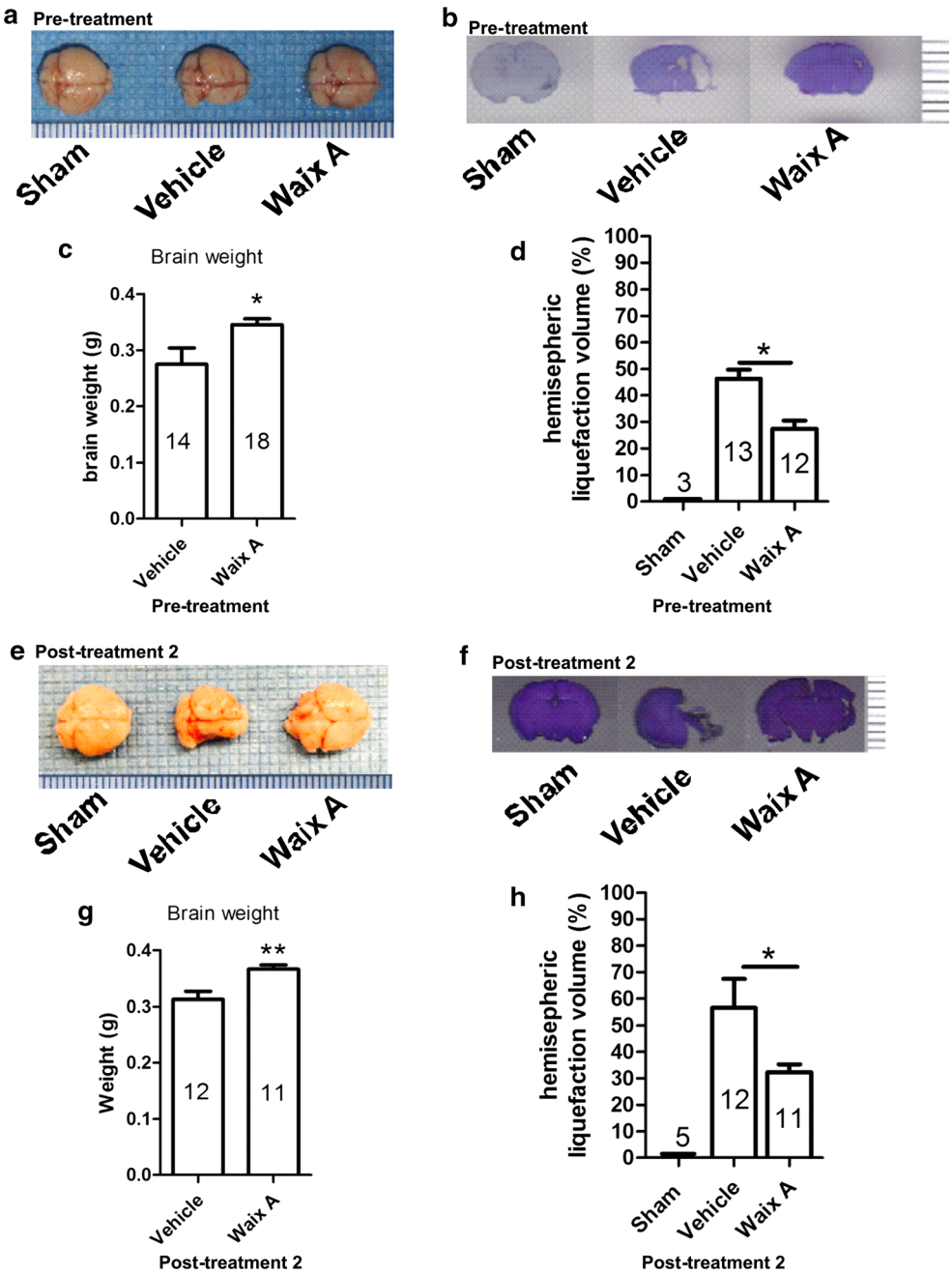

Fig. 5 Morphological assessment of brain injury 7 days after hypoxic-ischemic insult on neonatal brain. (**a**) Overall brain morphology is preserved in the pre-treatment paradigm 7 days after HI injury. (**b**) Nissl staining shows reduced liquefaction volume in waixenicin A-treated group in pre-treatment paradigm. (**c**) Brain weight is significantly higher in waixenicin A-treated group in pre-treatment paradigm (vehicle: 0.28 ± 0.03 g, $n = 14$; waixenicin A: 0.35 ± 0.01 g, $n = 18$, $p = 0.0146$). (**d**) Corrected ipsilateral liquefaction volume is significantly reduced in waixenicin A-treated group in pre-treatment paradigm (sham: 0, $n = 3$; vehicle: 46.3 ± 3.4%, $n = 13$; waixenicin A: 27.3 ± 3%, $n = 12$, $p < 0.0001$). (**e**) Overall brain morphology is preserved in the post-treatment 2 paradigm 7 days after HI injury. (**f**) Nissl staining shows reduced liquefaction volume in waixenicin A-treated group in post-treatment 2 paradigm. (**g**) Brain weight is significantly higher in waixenicin A-treated group in post-treatment 2 paradigm (vehicle: 0.32 ± 0.01 g, $n = 12$; waixenicin A: 0.38 ± 0.01 g, $n = 11$, $p = 0.0077$). (**h**) Corrected ipsilateral liquefaction volume is significantly reduced in waixenicin A-treated group in post-treatment 2 paradigm (sham: 0, $n = 5$; vehicle: 55.4 ± 6%, $n = 12$; waixenicin A: 34 ± 5%, $n = 11$, $p < 0.0001$). All data presented as mean ± SEM. Statistical analysis was done by Student *t* test or one-way ANOVA with Bonferroni post hoc (*$p < 0.05$)

0.3 s, $n = 12$ ($p = 0.0432$) (post-treatment (Fig. 6a, right) sham: 0.8 ± 0.07 s, $n = 14$; vehicle: 1.4 ± 0.01 s, $n = 23$; waixenicin A: 1.1 ± 0.06 s, $n = 25$, $p = 0.001$). Geotaxis reflex performance was also significantly improved in waixenicin A-treated group compared with that in the vehicle-treated group on day 1 (sham: 4.4 ± 0.4 s, $n = 8$; vehicle: 8.3 ± 1.3 s, $n = 13$; waixenicin A: 5.3 ± 0.4 s, $n = 12$, $p = 0.0461$) and day 3 (sham: 2.9 ± 0.3 s, $n = 8$; vehicle: 5.7 ± 0.7 s, n = 13; waixenicin A: 3.1 ± 0.3 s, $n = 12$, $p = 0.012$) post-HI in a pre-treatment paradigm (Fig. 6b, left), and on day 7 (sham: 2.4 ± 0.2 s, $n = 5$; vehicle: 4.1 ± 0.7 s, $n = 7$; waixenicin A: 3.5 ± 0.3 s, $n = 8$, $p < 0.0001$) in the post-treatment paradigm (Fig. 6b, right). Cliff avoidance reflex showed significant improvement in waixenicin A-treated group compared with that in the vehicle-treated group on day 1 (sham: 2.2 ± 0.2 s, $n = 8$; vehicle: 6.7 ± 1.5 s, $n = 13$; waixenicin A: 3.2 ± 0.4 s, $n = 12$, $p = 0.04$) and day 3 (sham: 1.7 ± 0.1 s, $n = 8$; vehicle: 4.5 ± 0.7 s, $n = 13$; waixenicin A: 2.9 ± 0.3 s, $n = 12$, $p = 0.021$) post-HI in the pre-treatment paradigm (Fig. 6c, left), and on day 7 (sham: 1.9 ± 0.2 s, $n = 5$; vehicle: 4.0 ± 0.5 s, $n = 7$; waixenicin A: 2.7 ± 0.4 s, $n = 8$, $p = 0.0132$) post-HI in the post-treatment paradigm (Fig. 6c, right). Grip strength was significantly improved with waixenicin A treatment on day 7 post-HI in both treatment paradigms (pre-treatment (Fig. 6d, left): sham: 22 ± 2.6, $n = 8$; vehicle: 9.4 ± 1 s, $n = 13$; waixenicin A: 20 ± 4.3 s,

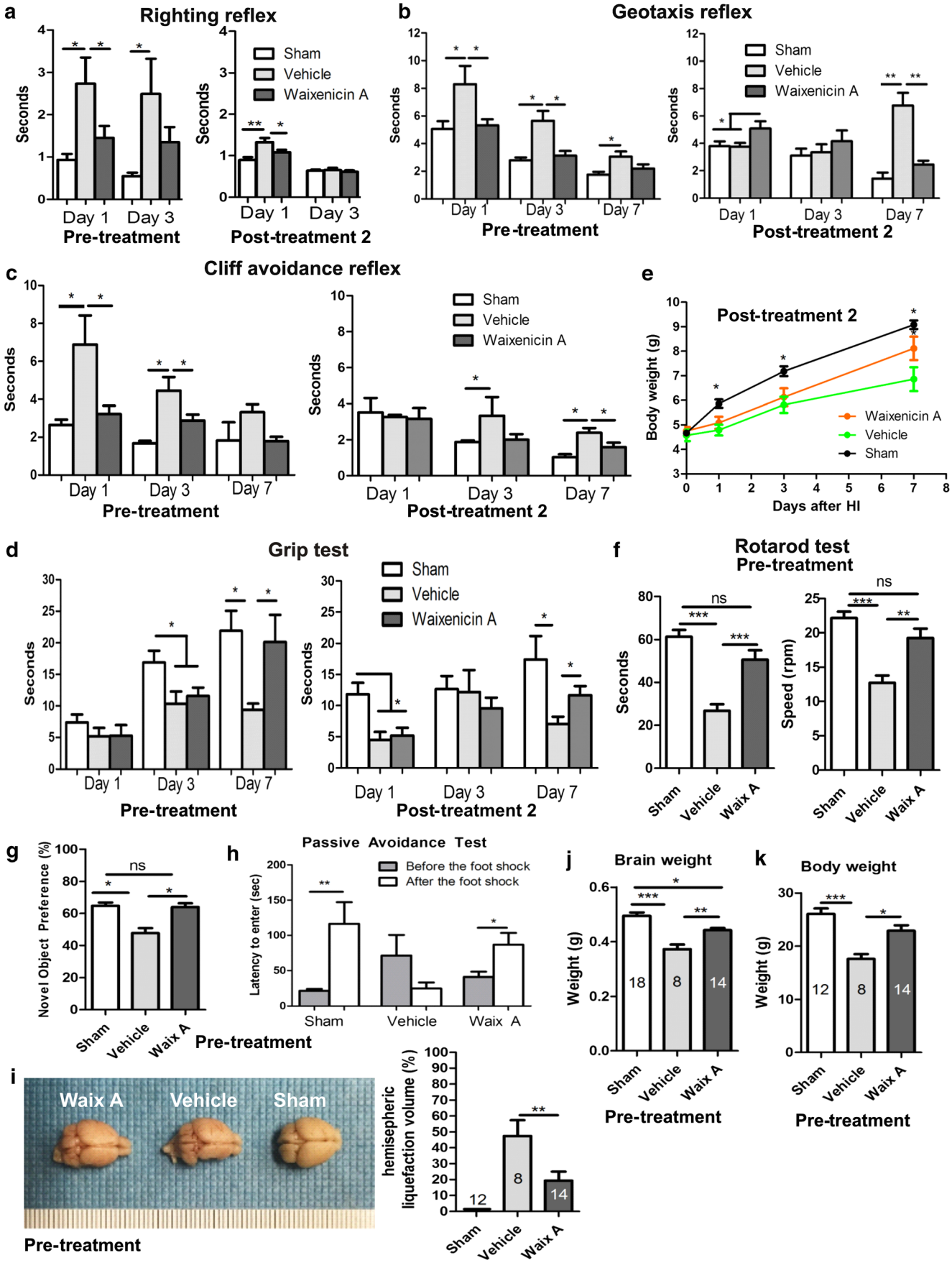
a
Righting reflex
Seconds
Day 1
Day 3
Pre-treatment
Sham
Vehicle
Waixenicin A
Post-treatment 2
b
Geotaxis reflex
Day 7
c
Cliff avoidance reflex
e
Post-treatment 2
Body weight (g)
Days after HI
d
Grip test
f
Rotarod test
Pre-treatment
Speed (rpm)
Sham
Vehicle
Waix A
g
Novel Object Preference (%)
h
Passive Avoidance Test
Before the foot shock
After the foot shock
Latency to enter (sec)
j
Brain weight
Weight (g)
k
Body weight
i
hemispheric liquefaction volume (%)

◀ **Fig. 6** Short (pre-treatment and post-treatment) and long-term (pre-treatment) behavioral assessment of functional recovery following hypoxic-ischemic injury. There was significant improvement in the following short-term neurobehavioral outcomes: (**a**) Righting reflex 1 day following HI injury in both paradigms (pre-treatment (control: $n = 8$, vehicle group: $n = 13$, waixenicin A group: $n = 12$) on the left ($p = 0.0432$), post-treatment 2 (control: $n = 14$, vehicle group: $n = 23$, waixenicin A group: $n = 25$) on the right ($p = 0.001$)); (**b**) geotaxis reflex 1 ($p = 0.0461$) and 3 days ($p = 0.012$) following HI injury in pre-treatment (control: $n = 8$, vehicle group: $n = 13$, waixenicin A group: $n = 12$) paradigm (left) and 7 days following HI injury in post-treatment 2 paradigm (control: $n = 5$, vehicle group: $n = 7$, waixenicin A group: $n = 8$) (right, $p < 0.0001$); (**c**) cliff avoidance reflex 1 day ($p = 0.04$) and 3 days ($p = 0.021$) following HI injury in pre-treatment (control: $n = 8$, vehicle group: $n = 13$, waixenicin A group: $n = 12$) paradigm (left) and 7 days following HI injury in post-treatment 2 (control: $n = 5$, vehicle group: $n = 7$, waixenicin A group: $n = 8$) paradigm (right, $p = 0.0132$); (**d**) grip test 7 days following HI injury in both paradigms (pre-treatment (control: $n = 8$, vehicle group: $n = 13$, waixenicin A group: $n = 12$) on the left ($p < 0.0001$), post-treatment 2 (control: $n = 5$, vehicle group: $n = 7$, waixenicin A group: $n = 8$) on the right ($p = 0.002$)); (**e**) body weight, as an indicator of recovery after HI, was found to be significantly higher in sham and waixenicin A-treated groups 7 days following HI injury in the post-treatment 2 paradigm (control: $n = 5$, vehicle group: $n = 7$, waixenicin A group: $n = 8$) ($p = 0.046$); (**f**) in the accelerated rotarod test, mice in waixenicin A-treated groups had a significantly improved motor and balance function as was evident by longer latency ($p < 0.0001$) and higher speed ($p < 0.0001$) at which waixenicin A-treated mice fell off the drum (control: $n = 12$, vehicle group: $n = 8$, waixenicin A group: $n = 14$); (**g**) in the novel object recognition test, mice in waixenicin A-treated groups had a significantly greater novel object preference (control: $n = 12$, vehicle group: $n = 8$, waixenicin A group: $n = 14$) ($p = 0.0002$); (**h**) in the passive avoidance test, waixenicin A-treated mice showed better memory function as was evident from significantly longer latency to enter the dark room 48 h after the foot shock (control: $n = 12$, vehicle group: $n = 8$, waixenicin A group: $n = 14$) ($p = 0.0009$); (**i**) overall brain morphology is preserved in waixenicin A-treated group, and liquefaction brain volume of waixenicin A-treated mice was significantly smaller 32 days after HI (control: $n = 12$, vehicle group: $n = 8$, waixenicin A group: $n = 14$) ($p < 0.0001$). Waixenicin A-treated mice had significantly greater (**j**) brain (control: $n = 18$, vehicle group: $n = 8$, waixenicin A group: $n = 14$) ($p < 0.0001$); (**k**) body weights (control: $n = 12$, vehicle group: $n = 8$, waixenicin A group: $n = 14$) ($p = 0.001$), indicating an enhanced general recovery in the long term. Note that (**j**) to (**k**) represented studies in the pre-treatment paradigm. All data presented as mean ± SEM. Statistical analysis: one-way ANOVA with Bonferroni post hoc, $^*p < 0.05$

$n = 12$, $p < 0.0001$; post-treatment (Fig. 6d, right): sham: 14 ± 1.7 s, $n = 5$; vehicle: 9.0 ± 1.0 s, $n = 7$; waixenicin A: 14 ± 2.1 s, $n = 8$, $p = 0.002$). Body weight of pups in the post-treatment paradigm was also measured as an indicator of recovery after HI. We found that 7 days after HI, the body weight of animals in sham and waixenicin A-treated groups was significantly higher than that of animals in vehicle-treated group (Fig. 6e) (sham: 9.1 ± 0.2 g, $n = 5$; vehicle: 6.9 ± 0.5 g, $n = 7$; waixenicin A: 8.1 ± 0.5 g, $n = 8$, $p = 0.046$).

These data demonstrate that waixenicin A treatment before and after the onset of hypoxia significantly improves functional recovery, as evident by improved performance on a battery of neurobehavioral tests.

Waixenicin A Improves Long-Term General and Functional Recovery and Preserves Overall Brain Morphology Following HI Injury

To determine whether waixenicin A treatment would also improve functional recovery in the long term, we subjected mice in the pre-treatment paradigm to accelerated rotarod test 4 weeks after HI injury. We found that mice in waixenicin A-treated groups had a significantly improved motor function, compared with vehicle-treated mice as was evident by longer latency (Fig. 6f, left: sham: 61 ± 3 s, $n = 12$; vehicle: 27 ± 3 s, $n = 8$; waixenicin A: 51 ± 4 s, $n = 14$, $p < 0.0001$) and higher speed (Fig. 6f, right: sham: 22 ± 1 rpm, $n = 12$; vehicle: 13 ± 1 rpm, $n = 8$; waixenicin A: 19 ± 1 rpm, $n = 14$, $p < 0.0001$) at which waixenicin A-treated mice fell off the drum.

To determine whether waixenicin A treatment attenuates memory impairment after HI [47, 48], we subjected mice in pre-treatment paradigm to passive avoidance test and novel object recognition test 4 weeks after HI injury. We found that mice in waixenicin A-treated groups had a significantly greater novel object preference, compared with vehicle-treated mice (Fig. 6g: % of time spent exploring both objects: sham: 65 ± 2%, $n = 12$; vehicle: 48 ± 3%, $n = 8$; waixenicin A: 64 ± 2%, $n = 14$, $p = 0.0002$). Waixenicin A-treated mice also showed better memory function compared with vehicle-treated mice, as was evident from significantly longer latency to enter the dark room 48 h after the foot shock (Fig. 6h: sham: 116 ± 31 s, $n = 12$; vehicle: 25 ± 9 s, $n = 8$; waixenicin A: 87 ± 17 s, $n = 14$, $p = 0.0009$).

Liquefaction brain volume of waixenicin A-treated mice was significantly smaller than that of vehicle-treated mice (Fig. 6i, right, % of ipsilateral hemisphere: sham: 0, $n = 12$; vehicle: 47 ± 10%, $n = 8$; waixenicin A: 19 ± 6%, $n = 14$, $p < 0.0001$). Representative images of brains extracted 32 days after HI procedure are shown in Fig. 6i, left. Waixenicin A-treated mice also had significantly greater brain weight (Fig. 6j: sham: 0.5 ± 0.01 g, $n = 18$; vehicle: 0.37 ± 0.02 g, $n = 8$; waixenicin A: 0.44 ± 0.01 g, $n = 14$, $p < 0.0001$) and body weight (Fig. 6k: sham: 26 ± 1 g, $n = 12$; vehicle: 18 ± 0.9 g, $n = 8$; waixenicin A: 23 ± 1 g, $n = 14$, $p = 0.001$), indicating an enhanced general recovery in the long term.

Overall, our data show that neurobehavioral deficits of neonatal HI injury persist in the long term and that waixenicin A treatment helps alleviate these motor and cognitive deficits.

Discussion

Here, we provide evidence that TRPM7 regulates cell death via calcium-dependent activation of calcineurin and CaMKII, and downstream signaling through p38, cofilin, and α-actinin in a mouse neonatal model of HIE. We used a novel, potent,

and specific pharmacological inhibitor of TRPM7 waixenicin A. We also evaluated waixenicin A as a potential treatment in a neonatal hypoxic-ischemic brain injury mouse model.

We have investigated proteomic changes in the brain following HI injury in vehicle-treated and waixenicin A-treated groups. Proteomic analyses following HI injury have been previously performed in several rodent models, and our findings were generally in agreement with published literature [49–52]. Since TRPM7 is a calcium-conducting channel, we focused on the proteins with molecular function of calcium binding. Among 18 identified proteins, Ca^{2+}/calmodulin-dependent protein kinase II (CaMKII), calmodulin and calcineurin were selected for further analysis due to their documented contribution to neuronal injury under pathological conditions [8–12, 53]. Moreover, upregulation of calcineurin expression following HI in our model has been consistent with a proteomic study on Wistar rat pups [49].

Further analysis of the downstream signaling of these proteins revealed that TRPM7 acts potentially through downstream signaling by p38, cofilin, and α-actinin-1. CaMKII, one of the most abundant protein kinases in the nervous system, plays a key role in synaptogenesis during development [54]. Our findings show a drastic depletion of CaMKII following HI, and a restoration of its expression following waixenicin A treatment, as supported by a previous report [55]. Ca^{2+} influx via *N*-methyl-D-aspartate (NMDA)-type glutamate receptors has long been considered a hallmark of excitotoxic neuronal injury during ischemic insults [56]. Binding of α-actinin, a protein that was upregulated in our model, to NMDA was shown to enhance activity of the receptor, while CAMKII binding attenuated the activity [57]. Moreover, actinin has been shown to play a role in transport of α-amino-3-hydroxy-5-methyl-4-isoxazole propionic acid (AMPA) receptors, well-known contributors to neuronal injury during stroke [58], to dendritic spines [59]. Additionally, CaMKII was shown to inhibit TRPM7 currents in hepatocytes [60]; however, this mechanism is yet to be confirmed in neurons. Together, these findings suggest that upregulation of actinin and downregulation of CaMKII, as seen in our study, may contribute to neuronal death and potential increase in TRPM7 activity and leave neurons vulnerable to further injurious stimuli. Waixenicin A treatment reduced actinin upregulation and restored CaMKII levels, thus conferring neuroprotection.

Calcineurin, Ca^{2+}/calmodulin-regulated phosphatase, has also been implicated in neuronal cell death under oxidative stress conditions [13–15]. In our study, we observed upregulation of calcineurin B (regulatory subunit) and calmodulin, suggesting an increase in calcineurin activity following HI. Waixenicin A treatment restored the levels of both proteins to sham levels. Similarly, activation of cofilin or actin depolymerizing factor (ADF) via dephosphorylation [61] has been linked to neuronal death under oxidative stress conditions, as well as blood–brain barrier disruption [62, 63]. It has been previously shown that CaMKII and calcineurin control cofilin activity via phosphorylation and dephosphorylation, respectively, through Ca^{2+}-dependent regulation of LIM-kinase1and phosphatase Slingshot-1L [64]. In our study, we observed a significant decrease in p-cofilin following HI injury, suggesting its upstream activation by calcineurin, while waixenicin A restored p-cofilin levels, potentially through restoring CaMKII expression and activity.

The role of p38 mitogen-activated protein kinase (p38 MAPK) in stroke has been controversial. While it has been reported that inhibition of p38 MAPK is neuroprotective against HI injury [65], another report suggested that activation of p38 MAPK reduced apoptotic cell death under HI conditions [66]. While it is possible that conflicting reports are due to differences in animal models and experimental conditions, in our model of neonatal HI, we observed a drastic decrease in p38 MAPK activation following HI, which was restored by waixenicin A treatment. Moreover, p38 activation was previously implicated in downstream reorganization of actin in endothelial cells [67] and neurons [68], and CaMKII was shown to be a potential activator of p38 [67]. A proposed signaling cascade of TRPM7-mediated neuronal cell death in neonatal HI is illustrated in Fig. 3 c [36, 42–44]. Together, our findings show that waixenicin A reduces brain injury through upstream regulation of actin stability, potentially affecting both neuronal and non-neuronal cells.

Nevertheless, although there may be consistency across cell types, it is important to note that the evidence supporting the sequential order of this cascade is demonstrated in different models. Here, we showed an involvement of TRPM7, CamKII, calcineurin, P38, and actinin in HI injury. However, future studies are necessary to verify the order of this signaling pathway in our current neonatal HI brain injury model. One approach is to inhibit the proposed proteins downstream of TRPM7 (e.g., pharmacologically with antagonists of CaMKII, calcineurin, p38 MAPK, and actinin).

Additionally, it remains elusive whether waixenicin A changes the expression levels of TRPM7 and the investigated downstream proteins in sham animals. Due to the relatively low TRPM7 activity in neurons under physiological conditions [4], it has been challenging to elucidate conclusively the effects of waixenicin A on TRPM7 and downstream protein markers using Western immunoblot. In our previous study [36], we showed that inhibiting TRPM7 in developing neurons with waixenicin A potentiated axonal outgrowth and branching in vitro. We speculate that this enhanced growth in cell cultures follows a similar mechanism of action as the one underlying the neuroprotective effects observed in the present study. That is, waixenicin A can potentially impact, in sham animals, the expression of TRPM7 and other investigated downstream proteins. In future studies, we aim to further elucidate this mechanism.

It has been previously demonstrated that growing axonal pathways are highly vulnerable to pathogenic factors such as HI. White matter injury is observed on MRI in 50% of premature infants [69, 70], while term infants with HIE predominantly exhibit watershed pattern of injury which includes white matter in the vascular boundary zones and extends into the cortical gray matter [71, 72]. In both cases, the myelination failure [73] and axonal damage [74] leave lasting neurological deficits and vulnerability to recurrent insults. While the direct link between TRPM7 activation and axonal degeneration is yet to be established, our previous study demonstrates that inhibition of TRPM7 activity using waixenicin A enhances axonal outgrowth and branching in developing neurons [36]. Oxidative stress, reactive oxygen species, and acidosis during HI create ideal conditions for TRPM7 activation [7] which could potentially disrupt the crucial patterns of axonal growth, thus exacerbating the extent of brain injury.

It is also important to note that TRPM7 expression has been confirmed in both neuronal and non-neuronal cells; therefore, the molecular pathway described above may not be limited to neurons only. TRPM7 expression has been shown in mouse cortical astrocytes. Silencing and pharmacological inhibition of TRPM7 in these cells impaired their proliferation and migration through via ERK and c-Jun N-terminal kinase (JNK) signaling, but not through p38 MAPK or Akt [66]. Additionally, TRPM7 currents have been demonstrated in anti-inflammatory microglia [75] and macrophages [76], where inhibition of TRPM7 activity reduced proliferation and migration of these cells.

Overall, inhibition of TRPM7 activity with waixenicin A in our model was beneficial and resulted in reduced infarct volume, preservation of neuronal numbers, reduction in apoptotic cell death, and preservation of short and long-term function. To further assess TRPM7 as a potential drug target to attenuate neonatal HI brain injury, future directions can evaluate other approaches of TRPM7 inhibition. Previously, we showed pharmacologically that the classical TRPM7 inhibitor carvacrol also had neuroprotective effects following neonatal HI injury [35]. However, the main concern when using carvacrol is its low specificity for TRPM7, which results in off-target effects [35]. The inhibitor employed in the present study, waixenicin A, is reported to be selective for TRPM7 in vitro [22]. Gene manipulation via knockdown of TRPM7 is also highly selective, which makes this approach a possible next step for future studies.

On a final note, in the current study, we focused on hippocampal neurons when conducting our in vitro assessments. Nonetheless, since HI affects the cortex as well as the hippocampus, future investigations should consider cortical neurons when examining effects of waixenicin A on cell death and TRPM7 activity. An in-depth understanding of the effects of TRPM7 inhibition on different cell types and their contribution to evolution of hypoxic-ischemic brain injury in vivo is required for complete evaluation of waixenicin A as a therapeutic tool.

Acknowledgments We thank S Huang for his technical assistance.

Funding Information This work was supported by the following grants: NIH NIGMS P20 (GM103466) to FDH; Hamamatsu/Queen's PET Imaging, LLC to AF; Natural Sciences and Engineering Research Council of Canada (NSERC) Discovery Grants to ZPF (RGPIN-2014-06471) and to HSS (RGPIN-2016-04574); NSERC Alexander Graham Bell Canada Graduate Scholarship to ET; NSERC Postgraduate Scholarship-Doctoral to RW.

Compliance with Ethical Standards

Conflict of Interest The authors declare that they have no conflict of interest.

Ethical Approval All applicable international, national, and institutional guidelines for the care and use of animals were followed. All procedures performed in studies involving animals were in accordance with Canadian Council on Animal Care guidelines and approved by University of Toronto Animal Care Committee. This article does not contain any studies with human participants performed by any of the authors.

References

1. Monica J. S. Nadler, Meredith C. Hermosura, Kazunori Inabe, Anne-Laure Perraud, Qiqin Zhu, Alexander J. Stokes, Tomohiro Kurosaki, Jean-Pierre Kinet, Reinhold Penner, Andrew M. Scharenberg, Andrea Fleig, LTRPC7 is a Mg·ATP-regulated divalent cation channel required for cell viability. Nature 411 2001;(6837):590–595.
2. Runnels LW, Yue L, Clapham DE. TRP-PLIK, a bifunctional protein with kinase and ion channel activities. Science. 2001;291:1043–7.
3. Monteilh-Zoller MK, Hermosura MC, Nadler MJ, Scharenberg AM, Penner R, Fleig A. TRPM7 provides an ion channel mechanism for cellular entry of trace metal ions. J Gen Physiol. 2003;121:49–60.
4. Sun H-S, Jackson MF, Martin LJ, Jansen K, Teves L, Cui H, et al. Suppression of hippocampal TRPM7 protein prevents delayed neuronal death in brain ischemia. Nat Neurosci. 2009;12:1300–7.
5. Landman N, Jeong SY, Shin SY, Voronov SV, Serban G, Kang MS, et al. Presenilin mutations linked to familial Alzheimer's disease cause an imbalance in phosphatidylinositol 4,5-bisphosphate metabolism. Proc Natl Acad Sci U S A. 2006;103:19524–9.
6. Coombes E, Jiang J, Chu XP, Inoue K, Seeds J, Branigan D, et al. Pathophysiologically relevant levels of hydrogen peroxide induce glutamate-independent neurodegeneration that involves activation of transient receptor potential melastatin 7 channels. Antioxid Redox Signal. 2011;14:1815–27.
7. Aarts M, Iihara K, Wei WL, Xiong ZG, Arundine M, Cerwinski W, et al. A key role for TRPM7 channels in anoxic neuronal death. Cell. 2003;115:863–77.
8. Hanson SK, Grotta JC, Waxham MN, Aronowski J, Ostrow P. Calcium/calmodulin-dependent protein kinase II activity in focal ischemia with reperfusion in rats. Stroke. 1994;25:466–73.
9. Hudmon A, Lebel E, Roy H, Sik A, Schulman H, Waxham MN, et al. A mechanism for Ca2+/calmodulin-dependent protein kinase

II clustering at synaptic and nonsynaptic sites based on self-association. J Neurosci. 2005;25:6971–83.
10. Waxham MN, Grotta JC, Silva AJ, Strong R, Aronowski J. Ischemia-induced neuronal damage: a role for calcium/calmodulin-dependent protein kinase II. J Cereb Blood Flow Metab. 1996;16:1–6.
11. Ashpole NM, Song W, Brustovetsky T, Engleman EA, Brustovetsky N, Cummins TR, et al. Calcium/calmodulin-dependent protein kinase II (CaMKII) inhibition induces neurotoxicity via dysregulation of glutamate/calcium signaling and hyperexcitability. J Biol Chem. 2012;287:8495–506.
12. Klug JR, Mathur BN, Kash TL, Wang HD, Matthews RT, Robison AJ, et al. Genetic inhibition of CaMKII in dorsal striatal medium spiny neurons reduces functional excitatory synapses and enhances intrinsic excitability. PLoS One. 2012;7:e45323.
13. Ankarcrona M, Dypbukt JM, Orrenius S, Nicotera P. Calcineurin and mitochondrial function in glutamate-induced neuronal cell death. FEBS Lett. 1996;394:321–4.
14. Asai A, Qiu J, Narita Y, Chi S, Saito N, Shinoura N, et al. High level calcineurin activity predisposes neuronal cells to apoptosis. J Biol Chem. 1999;274:34450–8.
15. See V, Loeffler JP. Oxidative stress induces neuronal death by recruiting a protease and phosphatase-gated mechanism. J Biol Chem. 2001;276:35049–59.
16. Bochelen D, Rudin M, Sauter A. Calcineurin inhibitors FK506 and SDZ ASM 981 alleviate the outcome of focal cerebral ischemic/reperfusion injury. J Pharmacol Exp Ther. 1999;288:653–9.
17. Kurinczuk JJ, White-Koning M, Badawi N. Epidemiology of neonatal encephalopathy and hypoxic-ischaemic encephalopathy. Early Hum Dev. 2010;86:329–38.
18. Lawn JE, Cousens S, Zupan J. 4 million neonatal deaths: when? Where? Why? Lancet. 2005;365:891–900.
19. Johnson AS, Mehl BT, Martin RS. Integrated hybrid polystyrene-polydimethylsiloxane device for monitoring cellular release with microchip electrophoresis and electrochemical detection. Anal Methods. 2015;7:884–93.
20. Perez A, Ritter S, Brotschi B, Werner H, Caflisch J, Martin E, et al. Long-term neurodevelopmental outcome with hypoxic-ischemic encephalopathy. J Pediatr. 2013;163:454–9.
21. Vannucci RC, Perlman JM. Interventions for perinatal hypoxic-ischemic encephalopathy. Pediatrics. 1997;100:1004–14.
22. Zierler S, Yao G, Zhang Z, Kuo WC, Porzgen P, Penner R, et al. Waixenicin A inhibits cell proliferation through magnesium-dependent block of transient receptor potential melastatin 7 (TRPM7) channels. J Biol Chem. 2011;286:39328–35.
23. Xu B, Xiao AJ, Chen W, Turlova E, Liu R, Barszczyk A, et al. Neuroprotective effects of a PSD-95 inhibitor in neonatal hypoxic-ischemic brain injury. Mol Neurobiol. 2016;53:5962–70.
24. Rice JE 3rd, Vannucci RC, Brierley JB. The influence of immaturity on hypoxic-ischemic brain damage in the rat. Ann Neurol. 1981;9:131–41.
25. Huang S, Turlova E, Li F, Bao M-H, Szeto V, Wong R, et al. Transient receptor potential melastatin 2 channels (TRPM2) mediate neonatal hypoxic-ischemic brain injury in mice. Exp Neurol. 2017;296:32–40.
26. Sun HS, Xu B, Chen W, Xiao A, Turlova E, Alibraham A, et al. Neuronal K_{ATP} channels mediate hypoxic preconditioning and reduce subsequent neonatal hypoxic-ischemic brain injury. Exp Neurol. 2015;263:161–71.
27. Vannucci RC, Vannucci SJ. Perinatal hypoxic-ischemic brain damage: evolution of an animal model. Dev Neurosci. 2005;27:81–6.
28. Yager JY, Ashwal S. Animal models of perinatal hypoxic-ischemic brain damage. Pediatr Neurol. 2009;40:156–67.
29. Bouet V, Freret T, Toutain J, Divoux D, Boulouard M, Schumann-Bard P. Sensorimotor and cognitive deficits after transient middle cerebral artery occlusion in the mouse. Exp Neurol. 2006;203:555–67.
30. Haelewyn B, Freret T, Pacary E, Schumann-Bard P, Boulouard M, Bernaudin M, et al. Long-term evaluation of sensorimotor and mnesic behaviour following striatal NMDA-induced unilateral excitotoxic lesion in the mouse. Behav Brain Res. 2007;178:235–43.
31. Ennaceur A, Delacour J. A new one-trial test for neurobiological studies of memory in rats. 1: behavioral data. Behav Brain Res. 1988;31:47–59.
32. Leger M, Quiedeville A, Bouet V, Haelewyn B, Boulouard M, Schumann-Bard P, et al. Object recognition test in mice. Nat Protoc. 2013;8:2531–7.
33. Sik A, Van NP, Prickaerts J, Blokland A. Performance of different mouse strains in an object recognition task. Behav Brain Res. 2003;147:49–54.
34. Huang S, Wang H, Turlova E, Abussaud A, Ji X, Britto LR, et al. GSK-3beta inhibitor TDZD-8 reduces neonatal hypoxic-ischemic brain injury in mice. CNS Neurosci Ther. 2017;23:405–15.
35. Chen W, Xu B, Xiao A, Liu L, Fang X, Liu R, et al. TRPM7 inhibitor carvacrol protects brain from neonatal hypoxic-ischemic injury. Mol Brain. 2015;8:11.
36. Turlova E, Bae CY, Deurloo M, Chen W, Barszczyk A, Horgen FD, et al. TRPM7 regulates axonal outgrowth and maturation of primary hippocampal neurons. Mol Neurobiol. 2016;53:595–610.
37. Nesvizhskii AI, Keller A, Kolker E, Aebersold R. A statistical model for identifying proteins by tandem mass spectrometry. Anal Chem. 2003;75:4646–58.
38. Ashburner M, Ball CA, Blake JA, Botstein D, Butler H, Cherry JM, et al. Gene ontology: tool for the unification of biology. The Gene Ontology Consortium. Nat Genet. 2000;25:25–9.
39. Oberg AL, Mahoney DW, Eckel-Passow JE, Malone CJ, Wolfinger RD, Hill EG, et al. Statistical analysis of relative labeled mass spectrometry data from complex samples using ANOVA. J Proteome Res. 2008;7:225–33.
40. Xin WK, Zhao XH, Xu J, Lei G, Kwan CL, Zhu KM, et al. The removal of extracellular calcium: a novel mechanism underlying the recruitment of N-methyl-D-aspartate (NMDA) receptors in neurotoxicity. Eur J Neurosci. 2005;21:622–36.
41. Szklarczyk D, Morris JH, Cook H, Kuhn M, Wyder S, Simonovic M, et al. The STRING database in 2017: quality-controlled protein-protein association networks, made broadly accessible. Nucleic Acids Res. 2017;45:D362–8.
42. Endres M, Fink K, Zhu J, Stagliano NE, Bondada V, Geddes JW, et al. Neuroprotective effects of gelsolin during murine stroke. J Clin Invest. 1999;103:347–54.
43. Kampfl A, Posmantur R, Nixon R, Grynspan F, Zhao X, Liu SJ, et al. mu-Calpain activation and calpain-mediated cytoskeletal proteolysis following traumatic brain injury. J Neurochem. 1996;67:1575–83.
44. Posmantur RM, Kampfl A, Liu SJ, Heck K, Taft WC, Clifton GL, et al. Cytoskeletal derangements of cortical neuronal processes three hours after traumatic brain injury in rats: an immunofluorescence study. J Neuropathol Exp Neurol. 1996;55:68–80.
45. Posmantur R, Kampfl A, Siman R, Liu J, Zhao X, Clifton GL, et al. A calpain inhibitor attenuates cortical cytoskeletal protein loss after experimental traumatic brain injury in the rat. Neuroscience. 1997;77:875–88.
46. Hofmann T, Schafer S, Linseisen M, Sytik L, Gudermann T, Chubanov V. Activation of TRPM7 channels by small molecules under physiological conditions. Pflugers Arch. 2014;466:2177–89.
47. Hattori K, Lee H, Hurn PD, Crain BJ, Traystman RJ, DeVries AC. Cognitive deficits after focal cerebral ischemia in mice. Stroke. 2000;31:1939–44.

48. Blasi F, Wei Y, Balkaya M, Tikka S, Mandeville JB, Waeber C, et al. Recognition memory impairments after subcortical white matter stroke in mice. Stroke. 2014;45:1468–73.
49. Rosenkranz K, May C, Meier C, Marcus K. Proteomic analysis of alterations induced by perinatal hypoxic-ischemic brain injury. J Proteome Res. 2012;11:5794–803.
50. Shao G, Wang Y, Guan S, Burlingame AL, Lu F, Knox R, et al. Proteomic analysis of mouse cortex postsynaptic density following neonatal brain hypoxia-ischemia. Dev Neurosci. 2017;39:66–81.
51. Hu X, Rea HC, Wiktorowicz JE, Perez-Polo JR. Proteomic analysis of hypoxia/ischemia-induced alteration of cortical development and dopamine neurotransmission in neonatal rat. J Proteome Res. 2006;5:2396–404.
52. Yang S, Yu M, Sun L, Xiao W, Yang X, Sun L, et al. Interferon-γ-induced intestinal epithelial barrier dysfunction by NF-κB/HIF-1α pathway. J Interf Cytokine Res. 2014;34:195–203.
53. Aronowski J, Grotta JC, Waxham MN. Ischemia-induced translocation of Ca2+/calmodulin-dependent protein kinase II: potential role in neuronal damage. J Neurochem. 1992;58:1743–53.
54. Rongo C, Kaplan JM. CaMKII regulates the density of central glutamatergic synapses in vivo. Nature. 1999;402:195–9.
55. Tang K, Liu C, Kuluz J, Hu B. Alterations of CaMKII after hypoxia-ischemia during brain development. J Neurochem. 2004;91:429–37.
56. Chen M, Lu TJ, Chen XJ, Zhou Y, Chen Q, Feng XY, et al. Differential roles of NMDA receptor subtypes in ischemic neuronal cell death and ischemic tolerance. Stroke. 2015;39:3042–8.
57. Leonard AS, Bayer KU, Merrill MA, Lim IA, Shea MA, Schulman H, et al. Regulation of calcium/calmodulin-dependent protein kinase II docking to N-methyl-D-aspartate receptors by calcium/calmodulin and alpha-actinin. J Biol Chem. 2002;277:48441–8.
58. Soundarapandian MM, Tu WH, Peng PL, Zervos AS, Lu Y. AMPA receptor subunit GluR2 gates injurious signals in ischemic stroke. Mol Neurobiol. 2005;32:145–55.
59. Schulz TW, Nakagawa T, Licznerski P, Pawlak V, Kolleker A, Rozov A, et al. Actin/alpha-actinin-dependent transport of AMPA receptors in dendritic spines: role of the PDZ-LIM protein RIL. J Neurosci. 2004;24:8584–94.
60. Mishra R, Rao V, Ta R, Shobeiri N, Hill CE. Mg^{2+}- and MgATP-inhibited and Ca^{2+}/calmodulin-sensitive TRPM7-like current in hepatoma and hepatocytes. Am J Physiol Gastrointest Liver Physiol. 2009;297:G687–94.
61. Suzuki K, Yamaguchi T, Tanaka T, Kawanishi T, Nishimaki-Mogami T, Yamamoto K, et al. Activation induces dephosphorylation of cofilin and its translocation to plasma membranes in neutrophil-like differentiated HL-60 cells. J Biol Chem. 1995;270:19551–6.
62. Alhadidi Q, Bin Sayeed MS, Shah ZA. Cofilin as a promising therapeutic target for ischemic and hemorrhagic stroke. Transl Stroke Res. 2016;7:33–41.
63. Alhadidi Q, Bin Sayeed MS, Shah ZA. The interplay between cofilin and phospho-cofilin: its role in maintaining blood brain barrier integrity. CNS Neurol Disord Drug Targets. 2017;16:279–90.
64. Zhao B, Tang H-L, Dan Q-Q, Zhao N, Liu J. Changes of BDNF expression in neurons in traumatic brain injury rats. Sichuan Da Xue Xue Bao Yi Xue Ban. 2012;43:236–9 249.
65. Hee HB, Choi J, Holtzman DM. Evidence that p38 mitogen-activated protein kinase contributes to neonatal hypoxic-ischemic brain injury. Dev Neurosci. 2002;24:405–10.
66. Pfeilschifter W, Czech B, Hoffmann BP, Sujak M, Kahles T, Steinmetz H, et al. Pyrrolidine dithiocarbamate activates p38 MAPK and protects brain endothelial cells from apoptosis: a mechanism for the protective effect in stroke? Neurochem Res. 2010;35:1391–401.
67. Nguyen A, Chen P, Cai H. Role of CaMKII in hydrogen peroxide activation of ERK1/2, p38 MAPK, HSP27 and actin reorganization in endothelial cells. FEBS Lett. 2004;572:307–13.
68. Correa SA, Eales KL. The role of p38 MAPK and its substrates in neuronal plasticity and neurodegenerative disease. J Signal Transduct. 2012;640979:1–12.
69. Miller SP, Ferriero DM, Leonard C, Piecuch R, Glidden DV, Partridge JC, et al. Early brain injury in premature newborns detected with magnetic resonance imaging is associated with adverse early neurodevelopmental outcome. J Pediatr. 2005;147:609–16.
70. Miller SP, Cozzio CC, Goldstein RB, Ferriero DM, Partridge JC, Vigneron DB, et al. Comparing the diagnosis of white matter injury in premature newborns with serial MR imaging and transfontanel ultrasonography findings. AJNR Am J Neuroradiol. 2003;24:1661–9.
71. Barkovich AJ, Hajnal BL, Vigneron D, Sola A, Partridge JC, Allen F, et al. Prediction of neuromotor outcome in perinatal asphyxia: evaluation of MR scoring systems. AJNR Am J Neuroradiol. 1998;19:143–9.
72. Sie LT, van der Knaap MS, Oosting J, de Vries LS, Lafeber HN, Valk J. MR patterns of hypoxic-ischemic brain damage after prenatal, perinatal or postnatal asphyxia. Neuropediatrics. 2000;31:128–36.
73. Segovia KN, McClure M, Moravec M, Luo NL, Wan Y, Gong X, et al. Arrested oligodendrocyte lineage maturation in chronic perinatal white matter injury. Ann Neurol. 2008;63:520–30.
74. Haynes RL, Billiards SS, Borenstein NS, Volpe JJ, Kinney HC. Diffuse axonal injury in periventricular leukomalacia as determined by apoptotic marker fractin. Pediatr Res. 2008;63:656–61.
75. Siddiqui T, Lively S, Ferreira R, Wong R, Schlichter LC. Expression and contributions of TRPM7 and $K_{Ca2.3}/SK_3$ channels to the increased migration and invasion of microglia in anti-inflammatory activation states. PLoS One. 2014;9:e106087.
76. Schilling T, Miralles F, Eder C. TRPM7 regulates proliferation and polarisation of macrophages. J Cell Sci. 2014;127:4561–6.